



HAL
open science

Full statistics of conjugated thermodynamic ensembles in chains of bistable units

Manon Benedito, Fabio Manca, Stefano Giordano

► **To cite this version:**

Manon Benedito, Fabio Manca, Stefano Giordano. Full statistics of conjugated thermodynamic ensembles in chains of bistable units. *Inventions*, 2019, 4 (1), pp.19. 10.3390/inventions4010019 . hal-02337961

HAL Id: hal-02337961

<https://hal.science/hal-02337961>

Submitted on 5 Oct 2020

HAL is a multi-disciplinary open access archive for the deposit and dissemination of scientific research documents, whether they are published or not. The documents may come from teaching and research institutions in France or abroad, or from public or private research centers.

L'archive ouverte pluridisciplinaire **HAL**, est destinée au dépôt et à la diffusion de documents scientifiques de niveau recherche, publiés ou non, émanant des établissements d'enseignement et de recherche français ou étrangers, des laboratoires publics ou privés.

Article

Full statistics of conjugated thermodynamic ensembles in chains of bistable units

Manon Benedito ^{1,‡}, Fabio Manca ^{2,‡} and Stefano Giordano ^{1,*}  0000-0003-4023-5384

¹ Institute of Electronics, Microelectronics and Nanotechnology CNRS-UMR 8520, Univ. Lille, Centrale Lille, ISEN, Univ. Valenciennes, LIA LICS/LEMAC, F-59000 Lille, France

² Laboratoire de Physique Statistique, Ecole Normale Supérieure, CNRS-UMR 8550, 75005 Paris, France

* Correspondence: stefano.giordano@univ.lille.fr

‡ These authors contributed equally to this work.

Version March 8, 2019 submitted to *Inventions*

Abstract: The statistical mechanics and the thermodynamics of small systems are characterized by the non-equivalence of the statistical ensembles. Concerning a polymer chain or an arbitrary chain of independent units, this concept leads to different force-extension responses for the isotensional (Gibbs) and the isometric (Helmholtz) thermodynamic ensembles for a limited number of units (far from the thermodynamic limit). While the average force-extension response has been largely investigated in both Gibbs and Helmholtz ensembles, the full statistical characterization of this thermo-mechanical behavior has not been approached by evaluating the corresponding probability densities. Therefore, we elaborate in this paper a technique for obtaining the probability density of the extension when the force is applied (Gibbs ensemble) and the probability density of the force when the extension is prescribed (Helmholtz ensemble). This methodology, here developed at thermodynamic equilibrium, is applied to a specific chain composed of units characterized by a bistable potential energy, which is able to mimic the folding and unfolding of several macromolecules of biological origin.

Keywords: small systems thermodynamics; Gibbs and Helmholtz ensembles; polymer chain; bistability; ensembles equivalence.

1. Introduction

The recent developments of thermodynamics and statistical mechanics concern the thermodynamics of small systems, kept far from the thermodynamic limit, and the stochastic thermodynamics, which is based on Langevin or stochastic differential equations. In the first theoretical approach, the small size of the system is carefully taken into account in order to analyze its effects on the overall behavior of the system [1,2] and, in particular, on the force-extension response in the case of macromolecular chains. One interesting feature of the small systems thermodynamics is the non-equivalence of the ensembles for finite sizes of the system, and the convergence to the equivalence of the ensembles in the thermodynamic limit [3–6]. In the second theoretical approach, the out-of-equilibrium statistical mechanics is introduced by means of the Langevin and Fokker-Planck equations, which represent the stochastic evolution of the phase-space variables and of their probability density, respectively [7–10]. In this context, the first and the second principles of the thermodynamics can be re-demonstrated [11–14] and other important fluctuation-dissipation theorems have been elaborated [15–21]. These results follow from the pioneering Sekimoto idea of the microscopic heat rate along a Brownian system trajectory [22,23]. Concerning the Brownian trajectory of a particle an interesting investigation concerns the generalization of the principle of the least action in a probabilistic situation, which is equivalent to the principle of maximization of uncertainty associated with the

33 stochastic motion [24]. Also, the well-known quantum uncertainty relation can be proved to hold
34 for non-quantum but stochastic trajectories of a Brownian particle [25]. Furthermore, the entropy
35 generation during the stochastic evolution of a system has been studied by means of the Gouy–Stodola
36 theorem [26] and applied to the biological context to model in original way molecular machines [27]
37 and to study the control and regulation of temperature in cells [28]. Other approaches for investigating
38 the behavior of molecular motors are based on the over-damped Langevin equation and have been
39 successfully compared to the experimental data of the F_1 -ATPase motor [29,30].

40 Nowadays, importantly, these theoretical approaches can be experimentally verified with the
41 employment of single-molecule devices (force spectroscopy), allowing the direct quantification of
42 the elasticity and the dynamical properties of individual macromolecules [31,32]. As a matter of
43 fact, specific devices like atomic-force microscopes, laser optical tweezers, magnetic tweezers and
44 micro-electro-mechanical systems [33–38] have been employed to investigate proteins [39–41], RNA
45 [42,43], and DNA [44–50].

46 Typically, the units or elements of polymers and of other macromolecules may exhibit a bistable
47 behavior or not, depending on their internal chemical structure. The general behavior and in particular
48 the force-extension response of chains without bistability is nowadays rather well understood [4,
49 51–54]. On the other hand, the complexity of chains with bistable units has been recently revealed
50 through force-spectroscopy experiments and is the subject of promising research efforts. Indeed, the
51 conformational transition between two states of each chain unit has been observed in polypeptides,
52 nucleic acids and other molecules. The possibility to measure the dynamic response of bistable
53 systems is very important for investigating the out-of-equilibrium statistical mechanics since the
54 coupling and/or the competition between the purely mechanical characteristic times and the chemical
55 characteristic times induced by the barrier separating the two states [55] can be directly probed and
56 compared with theoretical results (see, *e.g.*, [18,56,57]). Interestingly enough, for relatively short
57 bistable molecular chains, the applied boundary conditions play an important role in defining their
58 overall response [58–61].

59 The first boundary condition corresponds to experiments conducted at constant applied force. It
60 means that, in this case, one uses soft devices (low values of the intrinsic elastic constant of the devices)
61 and the experiments are called isotensional. This configuration corresponds to the Gibbs statistical
62 ensemble of the statistical mechanics, and leads to a plateau-like force-extension curve. The threshold
63 force related to this plateau must be interpreted by the synchronized transition of all the chain units
64 [46,62–67]. The second boundary condition corresponds to experiments conducted at prescribed
65 displacement. This situation can be obtained by hard devices (high values of the intrinsic elastic
66 constant of the devices) and experiments are called isometric. The process represents a realization of
67 the Helmholtz statistical ensemble of the statistical mechanics, and the corresponding force-extension
68 curve shows a sawtooth-like shape. This behavior proves that the units unfold sequentially in response
69 to the increasing extension [39,41,66–73]. In any case, the differences between isotensional and isometric
70 force-extension curves, or equivalently between Gibbs and Helmholtz ensembles, disappear if the
71 number of units is very large since, in the thermodynamic limit, the Gibbs and Helmholtz ensembles
72 are statistically equivalent, as largely discussed in the recent literature [3,6].

73 Typically in the theoretical analyses conducted to study the behavior of two-state systems under
74 isotensional or isometric conditions (see previous works), the considered quantities correspond to the
75 average values of the fluctuating variables. It means that one considers the average extension in the
76 Gibbs ensemble and the average force in the Helmholtz ensemble. However, it is important to study
77 the actual distributions of these fluctuating or stochastic variables in order to better understand the
78 random behavior of these systems and to draw more refined comparisons with experiments. Indeed,
79 it is important to underline that the experimental activities above outlined may probe not only the
80 average values of the relevant quantities but also their actual distribution. Basically, this is achieved by
81 a very large statistics of the trajectories of the system under investigation, which allows for a good
82 exploration of the phase space and, consequently, for the determination of the pertinent probability

83 densities. Therefore, in this paper we propose a methodology to determine the exact distributions or
84 probability densities of the pertinent quantities defined in both the Gibbs and the Helmholtz ensembles.
85 This methodology is developed here for systems at thermodynamic equilibrium, as discussed below.
86 In particular, for the Gibbs ensemble, we determine the distribution of the couple (\dot{x}_N, x_N) where
87 x_N is the extension of a chain of N bistable elements (under applied deterministic force), and, for
88 the Helmholtz ensemble, the distribution of (\dot{f}, f) where f is the measured force (under prescribed
89 deterministic extension). When the number of the units approaches infinity (thermodynamic limit),
90 the two ensembles become equivalent as previously stated [3,6]. This means that the force-extension
91 responses converge to the same curves. Conversely, the above defined probability densities are not the
92 same for $N \rightarrow \infty$ since they are defined through different variables and can not be directly compared.
93 The applied method is based on the spin variables approach, recently introduced to deal with bistable
94 or multistable systems at thermodynamic equilibrium. The idea based on the spin variables approach
95 consists in considering a discrete variable (or spin) associated to each bistable unit, able to define the
96 state of the unit itself. It means that an arbitrary bistable potential energy function describing a chain
97 unit can be reasonably approximated by two sping-like quadratic potentials representing the two wells
98 and, therefore, the switching between them is governed by the behavior of an ad-hoc discrete or spin
99 variable [74]. Of course, when we adopt the approximation of the energy wells with two quadratic
100 functions, we lose the information about the energy barrier between the wells and therefore we can
101 not use this version of our model to deal with out-of-equilibrium regimes [55]. This approach has
102 been recently used to investigate the properties of several two-state systems and macromolecular
103 chains [74–78]. Both the Gibbs and the Helmholtz ensembles can be studied by the spin variables
104 methodology, permitting to draw direct comparisons between isotensional and isometric conditions,
105 provided that we work at thermodynamic equilibrium. While the application of this technique to the
106 Gibbs ensemble is more direct since the integration of the partition functions can be typically performed
107 in closed form without particular difficulties, the approach used for the Helmholtz ensemble is more
108 involved. Indeed, in this case the partition function can not be directly integrated but it can be obtained
109 as Fourier transform of the Gibbs partition function, analytically continued on the complex plane. The
110 mathematical details about this idea can be found in Refs.[74–76]. In the present analysis, this approach
111 leads to closed form expressions for the probability densities defined above, and the final results can be
112 interpreted by introducing a form of duality between the two ensembles, useful to better understand
113 the specific features of the isotensional and isometric conditions. The system considered in this work is
114 quite simple and it should be viewed as a toy-model useful to better introduce the concepts and discuss
115 the results. Of course, this model and its analysis could be generalized by taking into account more
116 refined features (energy difference between the states, heterogeneity, two- or three-dimensionality,
117 cooperativity among the units and out-of-equilibrium evolution) in order to represent more realistic
118 systems. Here, we reduced the complexity as far as possible with the aim of presenting the adopted
119 methodology as effectively as possible.

120 It is interesting to remark that models based on bistable elements with statistical transitions
121 between the states have been also introduced to model plasticity, hysteretic behaviors and martensitic
122 transformations in solids [79–86]. Similar mathematical approaches are also applied to study phase
123 transforming cellular materials [87], band gap transmission in bistable systems [88], waves in bistable
124 lattices [89–91], and energy harvesting [92].

125 The structure of the paper is the following. In Section 2, we introduce the investigated model
126 and we determine the partition functions under both the Gibbs and the Helmholtz ensembles. Here,
127 we also discuss the force-extension relation for the two ensembles. In Section 3, we introduce the
128 complete probability density for the system in the whole phase space. This is a preliminary information
129 exploited afterwards to deal with the specific distributions of the two ensembles. Indeed, in Section 4,
130 we obtain the probability density of the couple (\dot{x}_N, x_N) versus f within the Gibbs ensemble, and in
131 Section 5, we get the probability density of the couple (\dot{f}, f) versus x_N within the Helmholtz ensemble.

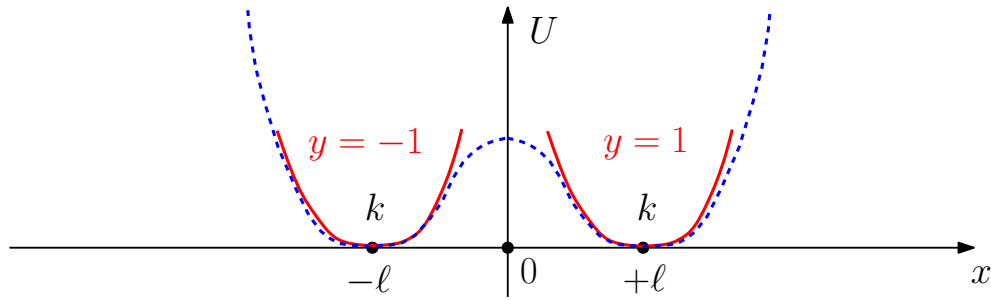


Figure 1. Bistable symmetric potential energy of a single domain (blue dashed line) and its approximation by means of four parabolic profiles (red solid lines).

132 A discussion concerning the duality and some conclusions on possible perspectives (Section 6) close
133 the paper.

134 2. Configurational partition functions and force-extension relations in Gibbs and Helmholtz 135 ensembles

136 The purpose of the present Section is to introduce a quite simple model which has the advantage
137 to be analytically solvable for both the Gibbs isotensional ensemble and the Helmholtz isometric
138 ensemble. The related mathematical analysis yields closed form expressions, which are beneficial to
139 the thorough understanding of the physics of bistability (or, more generally, multistability) in complex
140 systems, such as macromolecules of biological origin.

141 We consider a one-dimensional system composed of N elements with mechanical bistability,
142 connected in series to compose a chain. Each element of the chain is therefore represented by a
143 symmetric potential energy function $U(x)$ showing two minima at $x = \pm\ell$ (see Fig.1). As already
144 described in the Introduction, to perform an analysis of the system reduced to essentials, we introduce
145 a discrete variable y , which behaves as a spin, in place of considering the original bistable potential
146 function represented in Fig.1 (blue dashed line). This spin variable pertains to the phase space of the
147 system and, therefore, is a standard variable of the equilibrium statistical mechanics. The variable y
148 assumes its values in the set $\mathcal{S} = \{\pm 1\}$ and is used to identify the basin or well explored by the system.
149 In conclusion, the original bistable energy function is substituted with the simpler mathematical
150 expression

$$U(x, y) = \frac{1}{2}k(x - y\ell)^2. \quad (1)$$

151 The potential energy in Eq.(1), by varying the value of the spin variable in \mathcal{S} , generates the two
152 parabolic wells represented in Fig.1 (red solid lines). While without an applied stretching the units
153 are in each basin with the same probability (the average value of the end-to-end distance is zero), an
154 applied stretching induces a preferential direction in the extension of the chain. This stretching can be
155 applied by imposing a force f (positive or negative) or prescribing the position x_N of the last element
156 of the chain. Of course, in both cases, the first element is always tethered at the origin of the x -axis.
157 These two possible mechanisms of stretching generate different stochastic mechanical behaviors of the
158 system, which can be studied by calculating the corresponding configurational partition functions.

159 2.1. The Gibbs ensemble

160 In this case, we apply the force f to the last unit identified by its position x_N . The total potential
161 energy of the system under the Gibbs condition (isotensional ensemble) is therefore given by

$$U_{tot}^G(\vec{x}, \vec{y}; f) = \sum_{i=1}^N U(x_i - x_{i-1}, y_i) - f x_N, \quad (2)$$

162 where f is the force applied to the last element, $\vec{x} = (x_1, x_2, \dots, x_N)$ (continuous variables) and $\vec{y} =$
 163 (y_1, y_2, \dots, y_N) (discrete variables). For this system, we can define the configurational partition function
 164 Z_G , as follows

$$Z_G(f) = \sum_{y_1 \in \mathcal{S}} \dots \sum_{y_N \in \mathcal{S}} \int_{\mathbb{R}} \dots \int_{\mathbb{R}} e^{-\frac{U_{tot}^G}{k_B T}} dx_1 \dots dx_N, \quad (3)$$

165 where the variable \vec{x} is integrated whereas \vec{y} is summed. We can now substitute Eq.(2) in Eq.(3). To
 166 evaluate the integral we apply the change of variables $x_1 - x_0 = \zeta_1, x_2 - x_1 = \zeta_2, \dots, x_N - x_{N-1} = \zeta_N,$
 167 from which we get $x_N = \sum_{j=1}^N \zeta_j$ (with $x_0 = 0$). The change of variables within the multiple integral is
 168 implemented here by simply recalling that $d\vec{x} = J d\vec{\zeta}$. In this expression, the quantity J is the so-called
 169 Jacobian of the transformation defined as $J = |\det[\partial\vec{x}/\partial\vec{\zeta}]|$, where $[\partial\vec{x}/\partial\vec{\zeta}]_{ij}$ is the matrix of the first
 170 order partial derivatives $\partial x_i / \partial \zeta_j$. It can be easily proved that $J = 1$ for the proposed change of variables
 171 and, therefore, we finally get $d\vec{\zeta} = d\vec{x}$, which strongly simplifies the calculation. Hence, we get

$$Z_G(f) = \sum_{\vec{y} \in \mathcal{S}^N} \int_{\mathbb{R}^N} \exp \left\{ \sum_{j=1}^N \left[-\frac{U(\zeta_j; y_j)}{k_B T} + \frac{f \zeta_j}{k_B T} \right] \right\} d\vec{\zeta} = \left\{ \sum_{y \in \mathcal{S}} \mathcal{I}(y, f) \right\}^N, \quad (4)$$

172 where the integral $\mathcal{I}(y, f)$ is defined as

$$\mathcal{I}(y, f) = \int_{-\infty}^{+\infty} \exp \left[-\frac{k}{2k_B T} (\zeta - y\ell)^2 + \frac{f\zeta}{k_B T} \right] d\zeta, \quad (5)$$

173 and it can be calculated in closed form by means of the well-known expression

$$\int_{-\infty}^{+\infty} e^{-\alpha x^2} e^{\beta x} dx = \sqrt{\frac{\pi}{\alpha}} e^{\frac{\beta^2}{4\alpha}} \quad (\alpha > 0). \quad (6)$$

174 We eventually obtain the result

$$\mathcal{I}(y, f) = \sqrt{\frac{2\pi k_B T}{k}} \exp \left[\frac{y\ell f}{k_B T} + \frac{f^2}{2k_B T k} \right]. \quad (7)$$

175 Coming back to the configurational partition function, we have

$$Z_G(f) = \left\{ \sum_{y \in \mathcal{S}} \sqrt{\frac{2\pi k_B T}{k}} \exp \left[\frac{y\ell f}{k_B T} + \frac{f^2}{2k_B T k} \right] \right\}^N,$$

176 or, finally,

$$\boxed{Z_G(f) = \left(\frac{8\pi k_B T}{k} \right)^{\frac{N}{2}} \left\{ \exp \left(\frac{f^2}{2k_B T k} \right) \cosh \frac{\ell f}{k_B T} \right\}^N.} \quad (8)$$

177 It is important to remark that within the Gibbs ensemble the elements of the chain do not interact and
 178 this point leads to a configurational partition function which is in the form of a power with exponent
 179 N .

180 The extension of the chain can be directly calculated through the expression $x_N = -\partial U_{tot} / \partial f$
 181 and its average value is therefore $\langle x_N \rangle = \langle -\partial U_{tot} / \partial f \rangle$. It can be simply evaluated by means of the
 182 configurational partition function, as $\langle x_N \rangle = k_B T \partial / \partial f (\log Z_G)$. The calculation eventually gives

$$\boxed{\frac{\langle x_N \rangle}{N\ell} = \frac{f}{k\ell} + \tanh \left(\frac{\ell f}{k_B T} \right).} \quad (9)$$

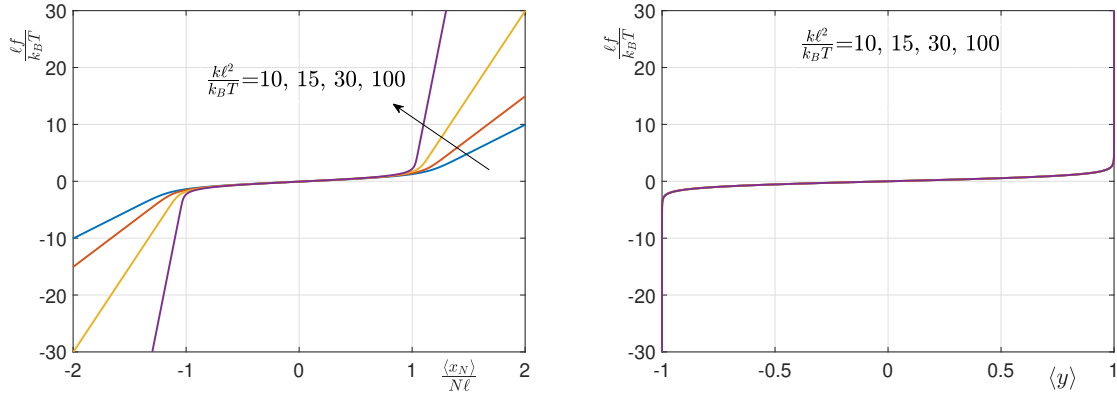


Figure 2. Average force-extension curves and average spin variables (plotted by means of dimensionless quantities) for the Gibbs ensemble with $N = 5$ and $\frac{k\ell^2}{k_B T} = 10, 15, 30, 100$.

183 We can also calculate the average value of the spin variable $\langle y \rangle = \langle y_i \rangle \forall i$, which is independent of the
 184 element considered in the chain and is given by

$$\langle y \rangle = \langle y_i \rangle = \tanh\left(\frac{\ell f}{k_B T}\right) \quad \forall i. \quad (10)$$

185 By combining Eq.(9) with Eq.(10), we immediately obtain $\frac{\langle x_N \rangle}{N\ell} = \frac{f}{k\ell} + \langle y \rangle$ or, equivalently,

$$f = k \left(\frac{\langle x_N \rangle}{N} - \ell \langle y \rangle \right). \quad (11)$$

186 This constitutive equation represents a spring-like behavior with an equilibrium length directly
 187 modulated by the average value of the spin variables.

188 An application of Eqs.(9) and (10) can be found in Fig.2. The force-extension curves have been
 189 plotted with dimensionless quantities and only one parameter defines the shape of the response, namely
 190 the elastic constant taken here into consideration through the dimensionless ratio $\frac{k\ell^2}{k_B T}$. It represents
 191 the ratio between the elastic (enthalpic) energy and the thermal energy. In these force-extension
 192 curves, we note a force plateau (for $f = 0$) corresponding to the synchronized switching (sometimes
 193 called cooperative) of the N units. This behavior is confirmed by the average spin variable (which
 194 is independent of $\frac{k\ell^2}{k_B T}$), showing a transition from -1 to $+1$, at the same threshold force $f = 0$ as
 195 the previously mentioned plateau. This force plateau is the classical result of force-spectroscopy
 196 experiments conducted with soft devices [62–67].

197 2.2. The Helmholtz ensemble

198 We can now introduce the second boundary condition corresponding to the Helmholtz ensemble.
 199 For imposing the isometric conditions, we consider the chain of bistable units with the two extremities
 200 tethered at the points $x_0 = 0$ and $x_N = x$, respectively. The total potential energy of the system can be
 201 therefore written as

$$U_{tot}^H(\vec{x}, \vec{y}; x_N) = \sum_{i=1}^N U(x_i - x_{i-1}, y_i), \quad (12)$$

202 where $x_N = x$ is the fixed extremity of the chain, $\vec{x} = (x_1, x_2, \dots, x_{N-1})$ (continuous variables) and
 203 $\vec{y} = (y_1, y_2, \dots, y_N)$ (discrete variables). In Eq.(12) the potential energy $U(x, y)$ of a single element is
 204 given in Eq.(1). The configurational partition function of this system can be written as

$$Z_H(x_N) = \sum_{y_1 \in \mathcal{S}} \dots \sum_{y_N \in \mathcal{S}} \int_{\mathfrak{R}} \dots \int_{\mathfrak{R}} e^{-\frac{U_{tot}^H}{k_B T}} dx_1 \dots dx_{N-1}. \quad (13)$$

205 It is now important to remark that the isometric condition $x_N = x$ impedes the direct evaluation of the
 206 integral in Eq.(13), which becomes considerably difficult. The solution to this problem can be found
 207 by drawing a comparison between Eqs.(3) and (13), eventually leading to the following important
 208 property: the two configurational partition functions Z_G and Z_H are related through a bilateral Laplace
 209 transform, as follows

$$Z_G(f) = \int_{-\infty}^{+\infty} Z_H(x) \exp\left(\frac{fx}{k_B T}\right) dx. \quad (14)$$

210 Moreover, if we let $f = -i\omega k_B T$, we simply obtain

$$Z_G(-i\omega k_B T) = \int_{-\infty}^{+\infty} Z_H(x) \exp(-i\omega x) dx, \quad (15)$$

211 which can be interpreted by affirming that the Fourier transform of Z_H gives the analytical continuation
 212 of Z_G on the imaginary axis of the complex plane. Exploiting this point, we can directly invert the
 213 Fourier transform, eventually obtaining

$$Z_H(x) = \frac{1}{2\pi} \int_{-\infty}^{+\infty} Z_G(-i\omega k_B T) \exp(i\omega x) d\omega. \quad (16)$$

214 Interestingly enough, we proved that the response of the system under the Helmholtz isometric
 215 ensemble can be analyzed through Eq.(16), which considers as a starting point, the configurational
 216 partition function of the Gibbs isotensional ensemble. Anyway, from Eq.(8), we have

$$Z_H(x) = \frac{1}{2\pi} \left(\frac{8\pi k_B T}{k}\right)^{\frac{N}{2}} \int_{-\infty}^{+\infty} \exp\left(-\frac{Nk_B T \omega^2}{2k}\right) \cos^N(\ell\omega) \exp(i\omega x) d\omega. \quad (17)$$

217 By using the Newton's Binomial Theorem

$$\cos^N x = \frac{1}{2^N} e^{-iNx} \sum_{t=0}^N \binom{N}{t} e^{2itx}, \quad (18)$$

218 we obtain from Eq.(17) the partial result

$$Z_H(x) = \frac{1}{2\pi} \left(\frac{8\pi k_B T}{k}\right)^{\frac{N}{2}} \frac{1}{2^N} \sum_{t=0}^N \binom{N}{t} \int_{-\infty}^{+\infty} \exp\left(-\frac{Nk_B T \omega^2}{2k}\right) \exp[i(x + 2t\ell - N\ell)\omega] d\omega. \quad (19)$$

219 To go further, the integral in Eq.(19) can be done with the help of the standard expression

$$\int_{-\infty}^{+\infty} e^{-\alpha x^2} e^{i\beta x} dx = \sqrt{\frac{\pi}{\alpha}} e^{-\frac{\beta^2}{4\alpha}} \quad (\alpha > 0), \quad (20)$$

220 eventually obtaining

$$Z_H(x) = \frac{1}{2\pi} \left(\frac{2\pi k_B T}{k}\right)^{\frac{N}{2}} \sum_{t=0}^N \binom{N}{t} \sqrt{\frac{2k\pi}{Nk_B T}} \exp\left[-\frac{k}{2Nk_B T} (x + 2t\ell - N\ell)^2\right]. \quad (21)$$

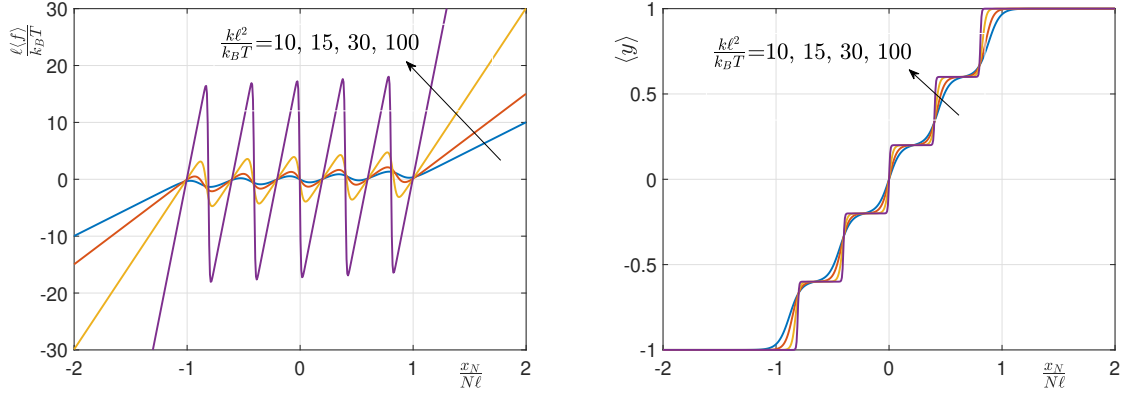


Figure 3. Average force-extension curves and average spin variables (plotted by means of dimensionless quantities) for the Helmholtz ensemble with $N = 5$ and $\frac{k\ell^2}{k_B T} = 10, 15, 30, 100$.

221 It is interesting to observe that the isometric configurational partition function here obtained can not
 222 be stated in power form (with exponent N). This point suggests that under the Helmholtz ensemble
 223 there is an effective interaction among the elements of the chain. The origin of this interaction is not
 224 explicitly defined in the potential energy of the system (i.e. in the bistable character of the units),
 225 but comes from the specific boundary conditions characterizing the Helmholtz ensemble. Indeed,
 226 the isometric conditions fix the end-to-end distance by generating an effective interaction among the
 227 extensions of the units.

228 Now, we can evaluate the average value of the overall force $\langle f \rangle = -k_B T \partial / \partial x (\log Z_H)$ applied to
 229 the system and the average value of the spin variables $\langle y \rangle = \left\langle \frac{1}{N} \sum_{i=1}^N y_i \right\rangle$ describing the transitions, as
 230 follows

$$\langle f \rangle = \frac{\sum_{t=0}^N \binom{N}{t} \frac{k}{N} (x + 2t\ell - N\ell) \exp \left[-\frac{k}{2Nk_B T} (x + 2t\ell - N\ell)^2 \right]}{\sum_{t=0}^N \binom{N}{t} \exp \left[-\frac{k}{2Nk_B T} (x + 2t\ell - N\ell)^2 \right]}, \quad (22)$$

231 and

$$\langle y \rangle = \frac{\frac{1}{N} \sum_{t=0}^N \binom{N}{t} (N - 2t) \exp \left[-\frac{k}{2Nk_B T} (x + 2t\ell - N\ell)^2 \right]}{\sum_{t=0}^N \binom{N}{t} \exp \left[-\frac{k}{2Nk_B T} (x + 2t\ell - N\ell)^2 \right]}. \quad (23)$$

232 An example of application of Eqs.(22) and (23) can be found in Fig.3, where we show the
 233 force extension response and the average spin variable for the Helmholtz ensemble. As before,
 234 the force-extension curves have been plotted with dimensionless quantities and only one parameter
 235 defines the shape of the response, namely the elastic constant taken here into consideration through
 236 the dimensionless ratio $\frac{k\ell^2}{k_B T}$. We observe that the force extension curve is composed of a number of
 237 peaks corresponding to the non-synchronized (sequential) switching of the units. Sometimes, this
 238 behavior is called non-cooperative in order to underline the independent transitions of the units. This
 239 is confirmed by the step-wise curve representing the average spin variable versus the chain extension.
 240 Each step corresponds to the switching of a unit induced by the increasing extension of the chain. This
 241 behavior agrees with previous theoretical and experimental results obtained with hard devices [66–73].

242 3. Complete probability densities in the Gibbs and Helmholtz ensembles

243 The results found in the previous Section concerning the Gibbs and Helmholtz partition functions
 244 and mechanical-configurational responses have been discussed for different systems in the scientific

245 literature concerning the thermodynamics of bistability and the folding-unfolding processes. As we
 246 will show below, they represent the basis for investigating the behavior of these systems in more detail.
 247 In particular, we are interested not only in the average value of the fluctuating quantities, but also in
 248 the comprehensive statistical behavior described by the complete probability densities. The knowledge
 249 of these more refined quantities allows for the determination of expected values of higher order such as
 250 variances, covariances and so on, very important to fully characterize the statistical properties of these
 251 systems. We define here the probability density of the system in the whole phase space within both the
 252 Gibbs and the Helmholtz statistical ensembles. These results will be used in the following Sections to
 253 find the probability density of the specific quantities characterizing the Gibbs and Helmholtz statistical
 254 ensembles.

255 Concerning the Gibbs ensemble, we can define the total energy of the system as

$$E_G(\vec{v}, \vec{x}, \vec{y}; f) = \sum_{i=1}^N \frac{1}{2} m v_i^2 + U_{tot}^G(\vec{x}, \vec{y}; f) = \sum_{i=1}^N \frac{1}{2} m v_i^2 + \sum_{i=1}^N U(x_i - x_{i-1}, y_i) - f x_N, \quad (24)$$

256 where v_i is the velocity of the i -th particle of the chain and $\vec{v}, \vec{x}, \vec{y} \in \mathfrak{R}^N$ while $f \in \mathfrak{R}$. The complete
 257 probability density in the phase space is therefore given by the canonical distribution

$$\rho_G(\vec{v}, \vec{x}, \vec{y}; f) = \frac{\exp\left[-\frac{1}{k_B T} E_G(\vec{v}, \vec{x}, \vec{y}; f)\right]}{\left(\sqrt{\frac{2\pi k_B T}{m}}\right)^N Z_G(f)}, \quad (25)$$

258 where the term $\left(\sqrt{\frac{2\pi k_B T}{m}}\right)^N$ has been added to normalize the kinetic part of the Boltzmann factor and
 259 the configurational partition function $Z_G(f)$ is given in Eq.(8). Of course, we have that

$$\sum_{\vec{y} \in \{-1, +1\}^N} \int_{\vec{x} \in \mathfrak{R}^N} \int_{\vec{v} \in \mathfrak{R}^N} \rho_G(\vec{v}, \vec{x}, \vec{y}; f) d\vec{v} d\vec{x} = 1 \forall f \in \mathfrak{R}. \quad (26)$$

260 Similarly, for the Helmholtz ensemble we can define the total energy as

$$E_H(\vec{v}, \vec{x}, \vec{y}; x_N) = \sum_{i=1}^{N-1} \frac{1}{2} m v_i^2 + U_{tot}^H(\vec{x}, \vec{y}; x_N) = \sum_{i=1}^{N-1} \frac{1}{2} m v_i^2 + \sum_{i=1}^N U(x_i - x_{i-1}, y_i), \quad (27)$$

261 where, as before, v_i is the velocity of the i -th particle of the chain and $\vec{v}, \vec{x} \in \mathfrak{R}^{N-1}$, $\vec{y} \in \mathfrak{R}^N$ while
 262 $x_N \in \mathfrak{R}$. In this case, the complete probability density in the phase space is given by the canonical
 263 distribution

$$\rho_H(\vec{v}, \vec{x}, \vec{y}; x_N) = \frac{\exp\left[-\frac{1}{k_B T} E_H(\vec{v}, \vec{x}, \vec{y}; x_N)\right]}{\left(\sqrt{\frac{2\pi k_B T}{m}}\right)^{N-1} Z_H(x_N)}, \quad (28)$$

264 where the term $\left(\sqrt{\frac{2\pi k_B T}{m}}\right)^{N-1}$ has been added to normalize the kinetic part of the Boltzmann factor
 265 and the configurational partition function $Z_H(x_N)$ is given in Eq.(21). Of course, we have that

$$\sum_{\vec{y} \in \{-1, +1\}^N} \int_{\vec{x} \in \mathfrak{R}^{N-1}} \int_{\vec{v} \in \mathfrak{R}^{N-1}} \rho_H(\vec{v}, \vec{x}, \vec{y}; x_N) d\vec{v} d\vec{x} = 1 \forall x_N \in \mathfrak{R}. \quad (29)$$

266 The two probability densities here described will be used to obtain a full statistics representing the
 267 behavior of the two isotensional and isometric ensembles.

268 4. Probability density of the couple (\dot{x}_N, x_N) versus f within the Gibbs ensemble

269 Since the force f is imposed within the Gibbs ensemble, we can measure the extension of the
 270 chain which is a random variable that must be defined by its probability density in order to have a
 271 complete description of its behavior. Here, for the sake of completeness, we elaborate the probability
 272 density $\varrho_G(\dot{x}_N, x_N; f)$ for the couple (\dot{x}_N, x_N) , where we defined $\dot{x}_N = v_N$. In this case, to obtain this
 273 probability density we have to sum or to integrate all the variables different from v_N and x_N in the
 274 complete density probability defined in Eq.(25). It means that we can write

$$\begin{aligned} \varrho_G(\dot{x}_N, x_N; f) &= \sum_{\vec{y} \in \{-1, +1\}^N} \int_{x_1} \dots \int_{x_{N-1}} \int_{v_1} \dots \int_{v_{N-1}} \rho_H(\vec{v}, \vec{x}, \vec{y}; x_N) dv_{N-1} \dots dv_1 dx_{N-1} \dots dx_1 \quad (30) \\ &= \sum_{\vec{y} \in \{-1, +1\}^N} \int_{x_1} \dots \int_{x_{N-1}} \int_{v_1} \dots \int_{v_{N-1}} \frac{\exp\left[-\frac{1}{k_B T} E_G(\vec{v}, \vec{x}, \vec{y}; f)\right]}{\left(\sqrt{\frac{2\pi k_B T}{m}}\right)^N Z_G(f)} dv_{N-1} \dots dv_1 dx_{N-1} \dots dx_1. \end{aligned}$$

275 Now, it is not difficult to recognize that the integral over the positions x_1, \dots, x_{N-1} immediately leads to
 276 the configurational partition function of the Helmholtz ensemble and the integral over the velocities
 277 v_1, \dots, v_{N-1} can be directly calculated with the classical Gaussian integral. Eventually, we obtain

$$\boxed{\varrho_G(\dot{x}_N, x_N; f) = \sqrt{\frac{m}{2\pi k_B T}} \exp\left(\frac{1}{2} m \dot{x}_N^2\right) \frac{\exp\left(\frac{f x_N}{k_B T}\right) Z_H(x_N)}{Z_G(f)}}. \quad (31)$$

278 This is the most important result of this section and represents the probability density of the couple
 279 (\dot{x}_N, x_N) for any value of the applied force f within the Gibbs ensemble.

280 We remark that this probability density can be factorized in two terms representing the density
 281 of \dot{x}_N and the density of x_N . The first factor simply corresponds to the Maxwell distribution for the
 282 one-dimensional velocity

$$\boxed{\varrho_G(\dot{x}_N) = \sqrt{\frac{m}{2\pi k_B T}} \exp\left(\frac{1}{2} m \dot{x}_N^2\right)}. \quad (32)$$

283 On the other hand, it is interesting to observe that the second configurational term depends on the
 284 ratio between the two partition functions

$$\boxed{\varrho_G(x_N; f) = \exp\left(\frac{f x_N}{k_B T}\right) \frac{Z_H(x_N)}{Z_G(f)}}. \quad (33)$$

285 This configurational density is correctly normalized because of the Laplace integral relationship
 286 between Gibbs and Helmholtz partition functions, reported in Eq.(14). The explicit form of
 287 $\varrho_G(\dot{x}_N, x_N; f)$ can be found by using the results given in Eqs.(8) and (21). The substitution yields
 288 the final expression

$$\boxed{\varrho_G(\dot{x}_N, x_N; f) = \sqrt{\frac{m}{2\pi k_B T}} \exp\left(\frac{1}{2} m \dot{x}_N^2\right) \frac{\frac{1}{2^N} \sum_{t=0}^N \binom{N}{t} \exp\left[-\frac{k}{2Nk_B T} (x_N + 2t\ell - N\ell)^2 + \frac{f x_N}{k_B T}\right]}{2\pi \sqrt{\frac{Nk_B T}{2k\pi}} \left\{ \exp\left(\frac{f^2}{2k_B T k}\right) \cosh \frac{\ell f}{k_B T} \right\}^N}}. \quad (34)$$

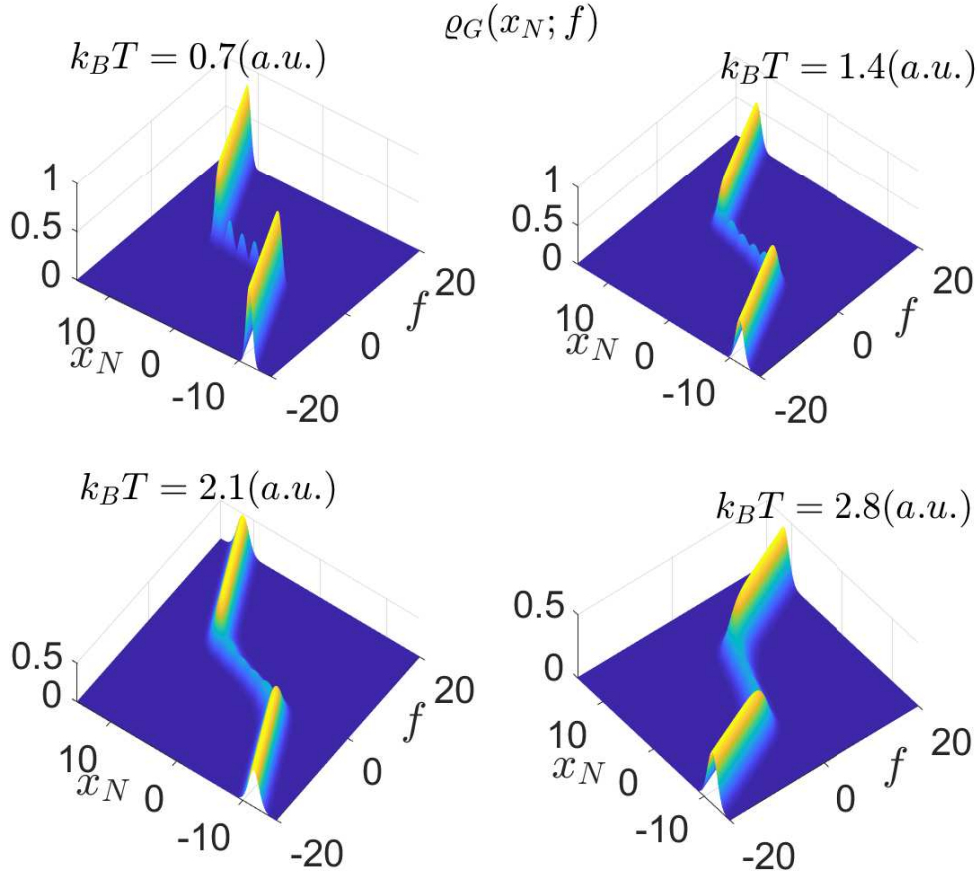


Figure 4. Three-dimensional representation of the Gibbs density $\rho_G(x_N; f)$ (see Eq.(33)) obtained with $N = 5$, $\ell = 1$ (a.u.), $k = 15$ (a.u.) and $k_B T = 0.7, 1.4, 2.1, 2.8$ (a.u.).

289 By means of this expression, we can give another proof of the result giving the average value of x_N .
 290 Indeed, we can write

$$\begin{aligned}
 \langle x_N \rangle &= \int_{-\infty}^{+\infty} \int_{-\infty}^{+\infty} x_N \rho_G(x_N, x_N; f) dx_N dx_N \\
 &= \int_{-\infty}^{+\infty} \int_{-\infty}^{+\infty} x_N \sqrt{\frac{m}{2\pi k_B T}} \exp\left(-\frac{1}{2} m \dot{x}_N^2\right) \frac{\exp\left(\frac{f x_N}{k_B T}\right) Z_H(x_N)}{Z_G(f)} dx_N dx_N \\
 &= \int_{-\infty}^{+\infty} \sqrt{\frac{m}{2\pi k_B T}} \exp\left(-\frac{1}{2} m \dot{x}_N^2\right) dx_N \int_{-\infty}^{+\infty} x_N \frac{\exp\left(\frac{f x_N}{k_B T}\right) Z_H(x_N)}{Z_G(f)} dx_N. \quad (35)
 \end{aligned}$$

291 Now, the first integral is equal to 1 and the second one can be elaborated as follows

$$\langle x_N \rangle = k_B T \frac{1}{Z_G(f)} \frac{\partial}{\partial f} \int_{-\infty}^{+\infty} \exp\left(\frac{f x_N}{k_B T}\right) Z_H(x_N) dx_N. \quad (36)$$

292 By using again the Laplace integral relation between Gibbs and Helmholtz partition functions, reported
 293 in Eq.(14), we easily get

$$\langle x_N \rangle = k_B T \frac{1}{Z_G(f)} \frac{\partial}{\partial f} Z_G(f) = k_B T \frac{\partial}{\partial f} \log Z_G(f), \quad (37)$$

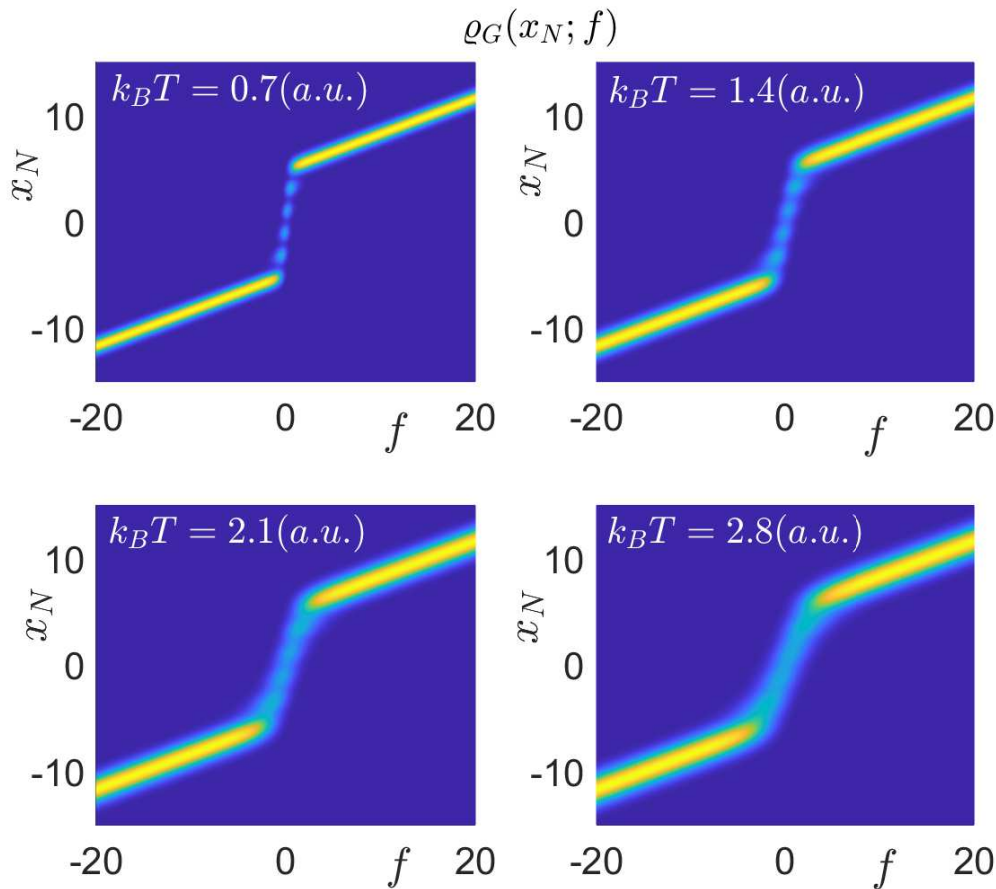


Figure 5. Two-dimensional representation of the Gibbs density $\rho_G(x_N; f)$ (see Eq.(33)) obtained with $N = 5$, $\ell = 1$ (a.u.), $k = 15$ (a.u.) and $k_B T = 0.7, 1.4, 2.1, 2.8$ (a.u.).

294 which is the well-known thermodynamic result.

295 An example of application of the results obtained in the present Section is given in Figs.4, 5, 6
 296 and 7. Since the kinetic component $\rho_G(\dot{x}_N)$ is simply given by the Maxwell distribution, we focus
 297 our attention to the configurational part given by $\rho_G(x_N; f)$. Accordingly, in Figs.4 and 5, we show a
 298 three-dimensional and a two-dimensional representation of the Gibbs density as function of x_N for
 299 a given applied force f . These results are represented for four different levels of thermal agitation
 300 in order to understand the effects of the disorder on the switching behavior between the states. The
 301 parameters used in this study are $N = 5$, $\ell = 1$ (a.u.), $k = 15$ (a.u.) and $k_B T = 0.7, 1.4, 2.1, 2.8$ (a.u.). It is
 302 interesting to observe that, in spite of the simple shape of the force-extension response characterized
 303 by a force plateau at $f = 0$ with a synchronized switching of the units, the probability density of the
 304 quantity x_N is multimodal for the force range characterizing the transition region. Indeed, in order to
 305 obtain the probability density of x_N for a given applied f we have to section the plots in Figs.4 and 5
 306 with a plane parallel to the x_N -axis and, at the same time, perpendicular to the f -axis. So doing, in the
 307 central transition region, we can observe the emergence of a series of peaks in the probability density
 308 confirming its multimodal character. This can be observed in Fig.6, where we plotted several curves
 309 $\rho_G(x_N; f)$ (see Eq.(33)), for different values of the applied force f . We can observe the symmetric and
 310 multimodal profile of the probability density for $f = 0$ (at the center of the transition region) and
 311 the asymmetric and monomodal shape of the density for a large applied force (out of the transition
 312 region). We remark the multimodal character of the probability density of x_N in spite of the simple
 313 force plateau observed in the force-extension response. To conclude this analysis, we underline that

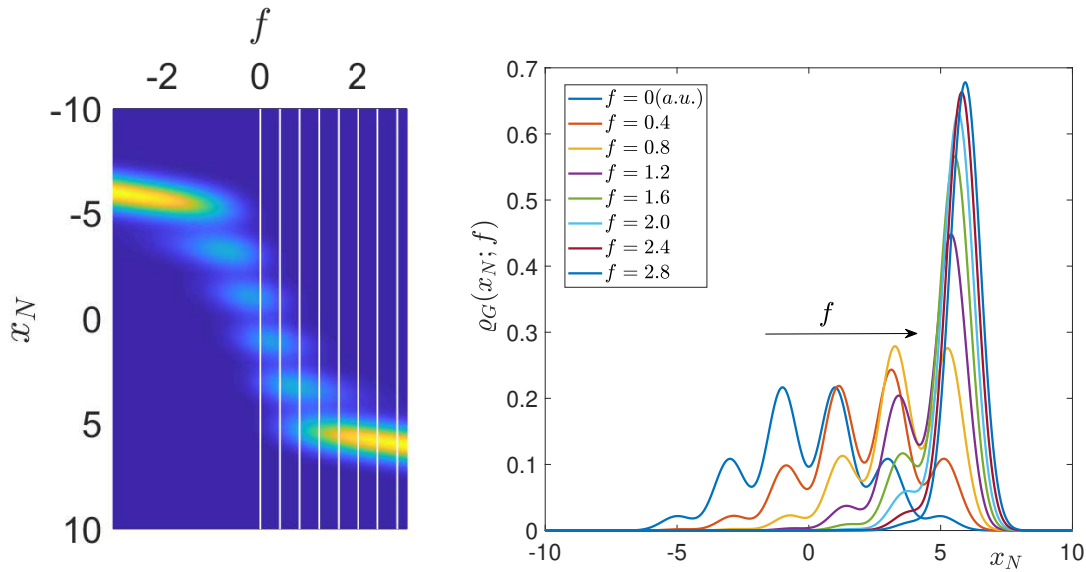


Figure 6. Examples of multimodal curves obtained through the Gibbs density $q_G(x_N; f)$ (see Eq.(33)). On the left panel, the two-dimensional representation of the Gibbs density is shown with the cuts corresponding to the curves plotted on the right panel. We used $N = 5$, $\ell = 1$ (a.u.), $k = 15$ (a.u.), $k_B T = 1$ (a.u.) and different values of the applied force f , as indicated in the legend.

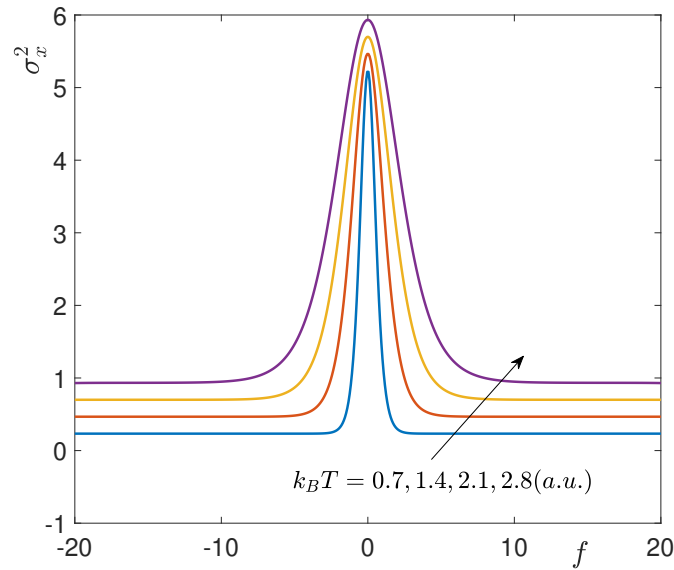


Figure 7. Variance of x_N obtained by the Gibbs density $q_G(x_N; f)$. As before, we used $N = 5$, $\ell = 1$ (a.u.), $k = 15$ (a.u.) and $k_B T = 0.7, 1.4, 2.1, 2.8$ (a.u.).

314 the knowledge of the full statistics for the system allows us to determine all possible expected values.
 315 As an example, we show in Fig.7 the behavior of the variance of the position in terms of the applied
 316 force f and the thermal energy $k_B T$. We note that the variance is higher in the transition region, where
 317 the two states of each unit can coexist. Moreover, we observe a larger variance for higher temperatures,
 318 as expected. Finally, we also note that the multimodal character of the probability density is smeared
 319 out by the integration process applied to calculate the variances. This behavior will be shown to be
 320 dual with respect to the Helmholtz ensemble response, which is the subject of the next Section.

321 5. Probability density of the couple (\dot{f}, f) versus x_N within the Helmholtz ensemble

322 The problem of finding the probability density for f and \dot{f} when x_N is imposed is more
 323 complicated since, in this case, the variables f and \dot{f} do not belong to the phase space and, therefore,
 324 we can not integrate the superfluous variables in order to get the searched density. To cope with this
 325 problem, we first introduce the standard technique to deal with a function of random variable. We
 326 suppose to have two random variables x and y , linked by a function $y = g(x)$. If $F_x(x)$ and $f_x(x)$
 327 are distribution function and probability density of the random variable x , we search for the same
 328 quantities $F_y(y)$ and $f_y(y)$ for $y = g(x)$. We use the symbol ξ for the elements of the probability space
 329 and we can write

$$F_x(x) = \Pr \{ \xi : x(\xi) \leq x \}, \quad (38)$$

330 and

$$f_x(x) = \frac{d}{dx} F_x(x). \quad (39)$$

331 Moreover, we can state that

$$\begin{aligned} F_y(y) &= \Pr \{ \xi : y(\xi) \leq y \} = \Pr \{ \xi : g(x(\xi)) \leq y \} \\ &= \int_{g(x) \leq y} f_x(x) dx = \int_{-\infty}^{+\infty} \mathbf{1}(y - g(x)) f_x(x) dx, \end{aligned} \quad (40)$$

332 where $\mathbf{1}(z)$ is the Heaviside step function. Therefore, we can obtain the probability density of $y = g(x)$
 333 by differentiation

$$\begin{aligned} f_y(y) &= \frac{d}{dy} F_y(y) \\ &= \frac{d}{dy} \int_{-\infty}^{+\infty} \mathbf{1}(y - g(x)) f_x(x) dx \\ &= \int_{-\infty}^{+\infty} \delta(y - g(x)) f_x(x) dx, \end{aligned} \quad (41)$$

334 where we have introduced the Dirac delta function $\delta(z)$. This method based on the delta functions can
 335 be used to approach the problem of finding the Helmholtz probability density. To apply this technique,
 336 we need to write the variables f and \dot{f} in terms of the variables of the phase space of the system. Given
 337 the total potential energy $U_{tot}^H(\vec{x}, \vec{y}; x_N) = \sum_{i=1}^N U(x_i - x_{i-1}, y_i)$, we can simply write

$$f = \frac{\partial U_{tot}^H}{\partial x_N} = k(x_N - x_{N-1} - y_N \ell) \quad (42)$$

338 and

$$\begin{aligned} \dot{f} &= \frac{d}{dt} \frac{\partial U_{tot}^H}{\partial x_N} = \sum_{i=1}^{N-1} \frac{\partial^2 U_{tot}^H}{\partial x_i \partial x_N} \frac{dx_i}{dt} \\ &= \sum_{i=1}^{N-1} \frac{\partial^2 U_{tot}^H}{\partial x_i \partial x_N} v_i = \frac{\partial^2 U_{tot}^H}{\partial x_{N-1} \partial x_N} v_{N-1} = -k v_{N-1} \end{aligned} \quad (43)$$

339 Now, given the complete probability density $\rho_H(\vec{v}, \vec{x}, \vec{y}; x_N)$, we can obtain the density for the desired
 340 variables f and \dot{f} as follows

$$\rho_H(\dot{f}, f; x_N) = \sum_{\vec{y}} \int_{\vec{x} \in \mathbb{R}^{N-1}} \int_{\vec{v} \in \mathbb{R}^{N-1}} \delta \left(f - \frac{\partial U_{tot}^H}{\partial x_N} \right) \delta \left(\dot{f} - \frac{\partial^2 U_{tot}^H}{\partial x_{N-1} \partial x_N} v_{N-1} \right) \rho_H(\vec{v}, \vec{x}, \vec{y}; x_N) d\vec{x} d\vec{v}. \quad (44)$$

341 This expression can be simplified delivering

$$\begin{aligned} \varrho_H(\dot{f}, f; x_N) &= \sum_{\vec{y}} \int_{\vec{x} \in \mathfrak{R}^{N-1}} \int_{\vec{v} \in \mathfrak{R}^{N-1}} \delta(f - kx_N + kx_{N-1} + ky_N \ell) \delta(\dot{f} + kv_{N-1}) \\ &\quad \times \frac{\exp\left[-\frac{1}{k_B T} E_H(\vec{v}, \vec{x}, \vec{y}; x_N)\right]}{\left(\sqrt{\frac{2\pi k_B T}{m}}\right)^{N-1} Z_H^N(x_N)} d\vec{x} d\vec{v}, \end{aligned} \quad (45)$$

342 where we used the notation $Z_H(x_N) = Z_H^N(x_N)$ in order to specify that the Helmholtz partition
 343 function corresponds to a system with N units. Indeed, in the following calculations, we will also need
 344 the same function calculated for a system with $N - 1$ units. The elaboration of $\varrho_H(\dot{f}, f; x_N)$ can be
 345 continued as follows

$$\begin{aligned} \varrho_H(\dot{f}, f; x_N) &= \frac{1}{\left(\sqrt{\frac{2\pi k_B T}{m}}\right)^{N-1} Z_H^N(x_N)} \\ &\quad \times \sum_{\vec{y}} \int_{\vec{x} \in \mathfrak{R}^{N-1}} \int_{\vec{v} \in \mathfrak{R}^{N-1}} \delta(f - kx_N + kx_{N-1} + ky_N \ell) \delta(\dot{f} + kv_{N-1}) \\ &\quad \times \exp\left(-\frac{m}{2k_B T} \sum_{i=1}^{N-1} v_i^2\right) \exp\left(-\frac{k}{2k_B T} \sum_{i=1}^N (x_i - x_{i-1} - y_i \ell)^2\right) d\vec{x} d\vec{v}, \quad (46) \\ &= \frac{1}{\left(\sqrt{\frac{2\pi k_B T}{m}}\right)^{N-1} Z_H^N(x_N)} \int_{\mathfrak{R}^{N-2}} \exp\left(-\frac{m}{2k_B T} \sum_{i=1}^{N-2} v_i^2\right) dv_1 \dots dv_{N-2} \\ &\quad \times \int_{\mathfrak{R}} \frac{1}{k} \delta\left(\frac{1}{k} \dot{f} + v_{N-1}\right) \exp\left(-\frac{m}{2k_B T} v_{N-1}^2\right) dv_{N-1} \\ &\quad \times \sum_{\vec{y}} \int_{\vec{x} \in \mathfrak{R}^{N-1}} \frac{1}{k} \delta\left(\frac{f}{k} - x_N + x_{N-1} + y_N \ell\right) \exp\left(-\frac{k}{2k_B T} \sum_{i=1}^{N-2} (x_i - x_{i-1} - y_i \ell)^2\right) \\ &\quad \times \exp\left(-\frac{k}{2k_B T} (x_{N-1} - x_{N-2} - y_{N-1} \ell)^2\right) \exp\left(-\frac{k}{2k_B T} (x_N - x_{N-1} - y_N \ell)^2\right) d\vec{x}, \quad (47) \end{aligned}$$

346 where we used the property $\delta(ax) = \frac{1}{|a|} \delta(x)$. We remember now that $\int_{-\infty}^{+\infty} \exp(-\alpha x^2) = \sqrt{\frac{\pi}{\alpha}}$ for $\alpha > 0$,
 347 we perform the integrals of the delta functions over v_{N-1} and x_{N-1} , and we get

$$\begin{aligned} \varrho_H(\dot{f}, f; x_N) &= \frac{1}{\sqrt{\frac{2\pi k_B T}{m}} Z_H^N(x_N)} \frac{1}{k} \exp\left(-\frac{m}{2k^2 k_B T} \dot{f}^2\right) \exp\left(-\frac{1}{2k k_B T} f^2\right) \\ &\quad \times \sum_{\vec{y}} \int_{\vec{x} \in \mathfrak{R}^{N-2}} \frac{1}{k} \exp\left(-\frac{k}{2k_B T} \sum_{i=1}^{N-2} (x_i - x_{i-1} - y_i \ell)^2\right) \\ &\quad \times \exp\left(-\frac{k}{2k_B T} (x_N - \frac{1}{k} \dot{f} - y_N \ell - x_{N-2} - y_{N-1} \ell)^2\right) dx_1 \dots dx_{N-2}. \quad (48) \end{aligned}$$

348 We can now recall the explicit definition of $Z_H^N(x_N)$ (see Eq.(13)), and we also introduce the exact
349 expression for $Z_H^{N-1}(x_{N-1})$

$$Z_H^N(x_N) = \sum_{y_1 \in \mathcal{S}} \dots \sum_{y_N \in \mathcal{S}} \int_{\mathbb{R}} \dots \int_{\mathbb{R}} \exp\left(-\frac{k}{2k_B T} \sum_{i=1}^N (x_i - x_{i-1} - y_i \ell)^2\right) dx_1 \dots dx_{N-1}, \quad (49)$$

$$Z_H^{N-1}(x_{N-1}) = \sum_{y_1 \in \mathcal{S}} \dots \sum_{y_{N-1} \in \mathcal{S}} \int_{\mathbb{R}} \dots \int_{\mathbb{R}} \exp\left(-\frac{k}{2k_B T} \sum_{i=1}^{N-1} (x_i - x_{i-1} - y_i \ell)^2\right) dx_1 \dots dx_{N-2}. \quad (50)$$

350 So, in Eq.(48), we can identify the partition function $Z_H^{N-1}(x_{N-1})$ calculated for $x_{N-1} = x_N - \frac{1}{k}f - y_N \ell$,
351 by obtaining

$$\begin{aligned} \varrho_H(\dot{f}, f; x_N) &= \frac{1}{k^2 \sqrt{\frac{2\pi k_B T}{m}}} \exp\left(-\frac{m}{2k^2 k_B T} \dot{f}^2\right) \exp\left(-\frac{1}{2k k_B T} f^2\right) \\ &\quad \times \frac{\sum_{y_N} Z_H^{N-1}\left(x_N - \frac{1}{k}f - y_N \ell\right)}{Z_H^N(x_N)}, \end{aligned} \quad (51)$$

or, equivalently,

$$\begin{aligned} \varrho_H(\dot{f}, f; x_N) &= \frac{1}{k^2 \sqrt{\frac{2\pi k_B T}{m}}} \exp\left(-\frac{m}{2k^2 k_B T} \dot{f}^2\right) \exp\left(-\frac{1}{2k k_B T} f^2\right) \\ &\quad \times \frac{Z_H^{N-1}\left(x_N - \frac{1}{k}f - \ell\right) + Z_H^{N-1}\left(x_N - \frac{1}{k}f + \ell\right)}{Z_H^N(x_N)}. \end{aligned} \quad (52)$$

352 This is the final result for the probability density within the Helmholtz ensemble. It is interesting
353 to observe that it can be written in terms of the two partition functions $Z_H^N(x_N)$ and $Z_H^{N-1}(x_{N-1})$,
354 corresponding to systems of size N and $N - 1$, respectively.

355 We can split this probability density in two independent components describing separately \dot{f} and
356 f , as follows

$$\varrho_H(\dot{f}) = \frac{1}{k \sqrt{\frac{2\pi k_B T}{m}}} \exp\left(-\frac{m}{2k^2 k_B T} \dot{f}^2\right), \quad (53)$$

357

$$\varrho_H(f; x_N) = \frac{1}{k} \exp\left(-\frac{1}{2k k_B T} f^2\right) \frac{Z_H^{N-1}\left(x_N - \frac{1}{k}f - \ell\right) + Z_H^{N-1}\left(x_N - \frac{1}{k}f + \ell\right)}{Z_H^N(x_N)}, \quad (54)$$

358 and we can prove the normalization of the two results. For the first density function $\varrho_H(\dot{f})$, the
359 normalization directly comes from the classical integral $\int_{-\infty}^{+\infty} \exp(-\alpha x^2) = \sqrt{\frac{\pi}{\alpha}}$ for $\alpha > 0$. For proving
360 the normalization of the second density function $\varrho_H(f; x_N)$, we have to study the integral

$$\int_{-\infty}^{+\infty} \exp\left(-\frac{1}{2k k_B T} f^2\right) \left[Z_H^{N-1}\left(x_N - \frac{1}{k}f - \ell\right) + Z_H^{N-1}\left(x_N - \frac{1}{k}f + \ell\right) \right] df. \quad (55)$$

361 To do this, we observe that from Eqs.(49) and (50) we easily get the relation

$$Z_H^N(x) = \sum_y \int_{-\infty}^{+\infty} Z_H^{N-1}(\eta) \exp\left(-\frac{k}{2k_B T} \sum_{i=1}^N (x - \eta - y \ell)^2\right) d\eta, \quad (56)$$

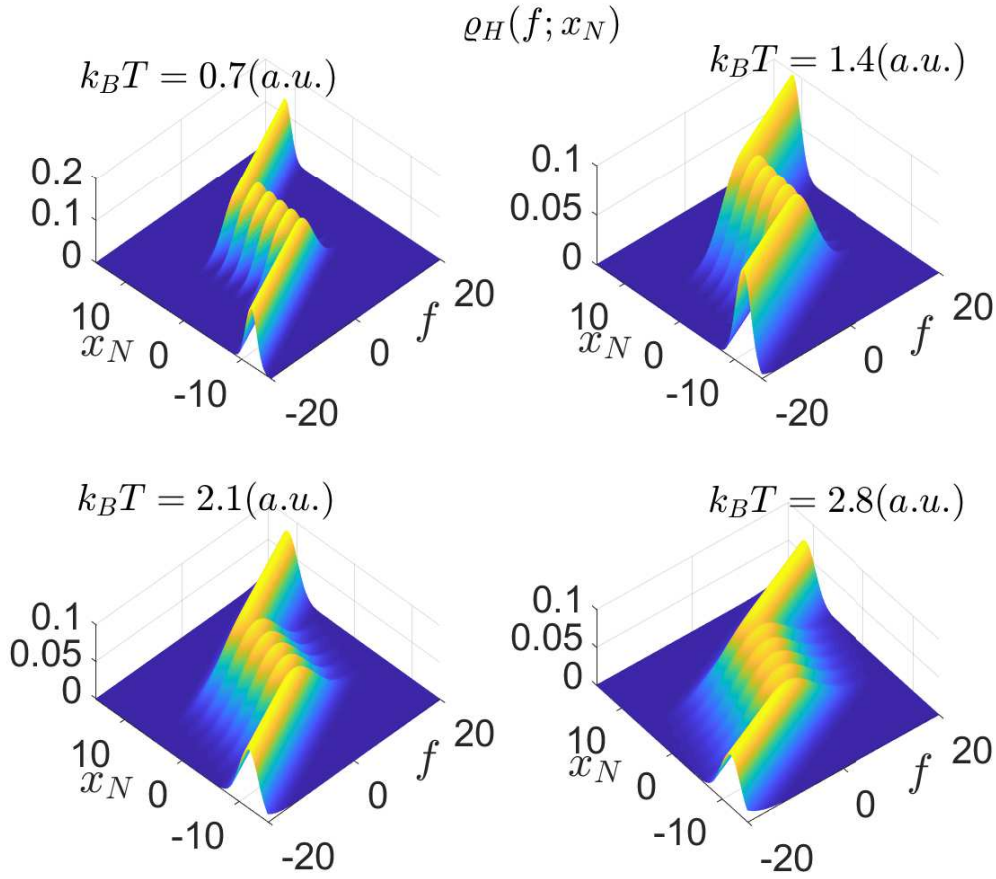


Figure 8. Three-dimensional representation of the Helmholtz density $\rho_H(f; x_N)$ (see Eq.(54)) obtained with $N = 5$, $\ell = 1$ (a.u.), $k = 15$ (a.u.) and $k_B T = 0.7, 1.4, 2.1, 2.8$ (a.u.).

362 which can be also written as

$$Z_H^N(x) = \int_{-\infty}^{+\infty} Z_H^{N-1}(\eta_a) \exp\left(-\frac{k}{2k_B T} \sum_{i=1}^N (x - \eta_a - \ell)^2\right) d\eta_a \quad (57)$$

$$+ \int_{-\infty}^{+\infty} Z_H^{N-1}(\eta_b) \exp\left(-\frac{k}{2k_B T} \sum_{i=1}^N (x - \eta_b + \ell)^2\right) d\eta_b. \quad (58)$$

363 We can then make the changes of variables $\eta_a + \ell = \xi$ and $\eta_b - \ell = \xi$, leading to

$$Z_H^N(x) = \int_{-\infty}^{+\infty} \exp\left[-\frac{k}{2k_B T} (x - \xi)^2\right] \left[Z_H^{N-1}(\xi - \ell) + Z_H^{N-1}(\xi + \ell) \right] d\xi. \quad (59)$$

364 Now, by letting $x - \xi = f/k$ we eventually obtain that

$$Z_H^N(x) = \frac{1}{k} \int_{-\infty}^{+\infty} \exp\left(-\frac{1}{2kk_B T} f^2\right) \left[Z_H^{N-1}\left(x_N - \frac{1}{k}f - \ell\right) + Z_H^{N-1}\left(x_N - \frac{1}{k}f + \ell\right) \right] df. \quad (60)$$

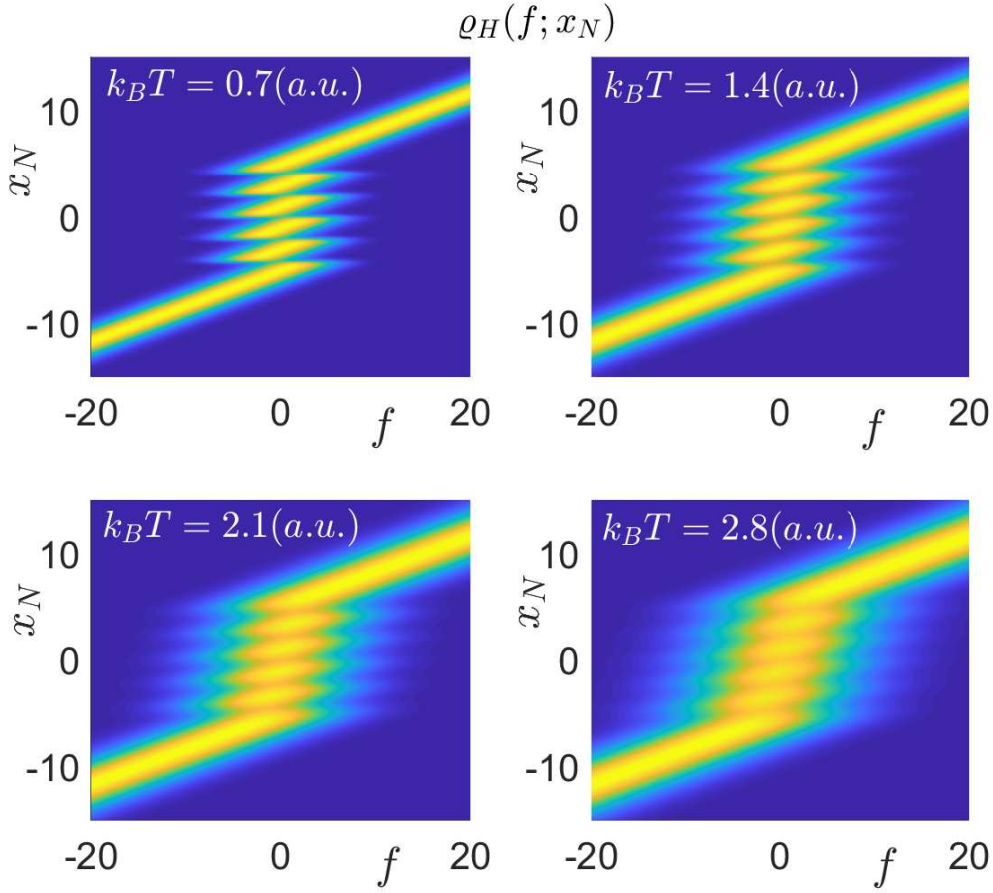


Figure 9. Two-dimensional representation of the Helmholtz density $\varrho_H(f; x_N)$ (see Eq.(54)) obtained with $N = 5$, $\ell = 1$ (a.u.), $k = 15$ (a.u.) and $k_B T = 0.7, 1.4, 2.1, 2.8$ (a.u.).

365 Finally, this result proves that $\varrho_H(f; x_N)$ is correctly normalized, being true that $\int_{-\infty}^{+\infty} \varrho_H(f; x_N) df = 1$.
 366 We also prove that we can re-obtain the well known expression for the average value of the force in the
 367 Helmholtz ensemble. To do this we consider the expression

$$\langle f \rangle = \int_{-\infty}^{+\infty} f \varrho_H(f; x_N) df \quad (61)$$

$$= \frac{1}{k} \int_{-\infty}^{+\infty} f \exp\left(-\frac{1}{2kk_B T} f^2\right) \frac{Z_H^{N-1}\left(x_N - \frac{1}{k}f - \ell\right) + Z_H^{N-1}\left(x_N - \frac{1}{k}f + \ell\right)}{Z_H^N(x_N)} df, \quad (62)$$

368 and we apply the change of variable $x_N - f/k = \xi$ leading to

$$\begin{aligned} \langle f \rangle &= k \int_{-\infty}^{+\infty} (x_N - \xi) \exp\left(-\frac{k}{2k_B T} (x_N - \xi)^2\right) \frac{Z_H^{N-1}(\xi - \ell) + Z_H^{N-1}(\xi + \ell)}{Z_H^N(x_N)} d\xi \\ &= -k_B T \frac{1}{Z_H^N(x_N)} \frac{\partial}{\partial x_N} \int_{-\infty}^{+\infty} \exp\left(-\frac{k}{2k_B T} (x_N - \xi)^2\right) \left[Z_H^{N-1}(\xi - \ell) + Z_H^{N-1}(\xi + \ell)\right] d\xi \\ &= -k_B T \frac{1}{Z_H^N(x_N)} \frac{\partial}{\partial x_N} Z_H^N(x_N) \\ &= -k_B T \frac{\partial}{\partial x_N} \log Z_H^N(x_N) \end{aligned} \quad (63)$$

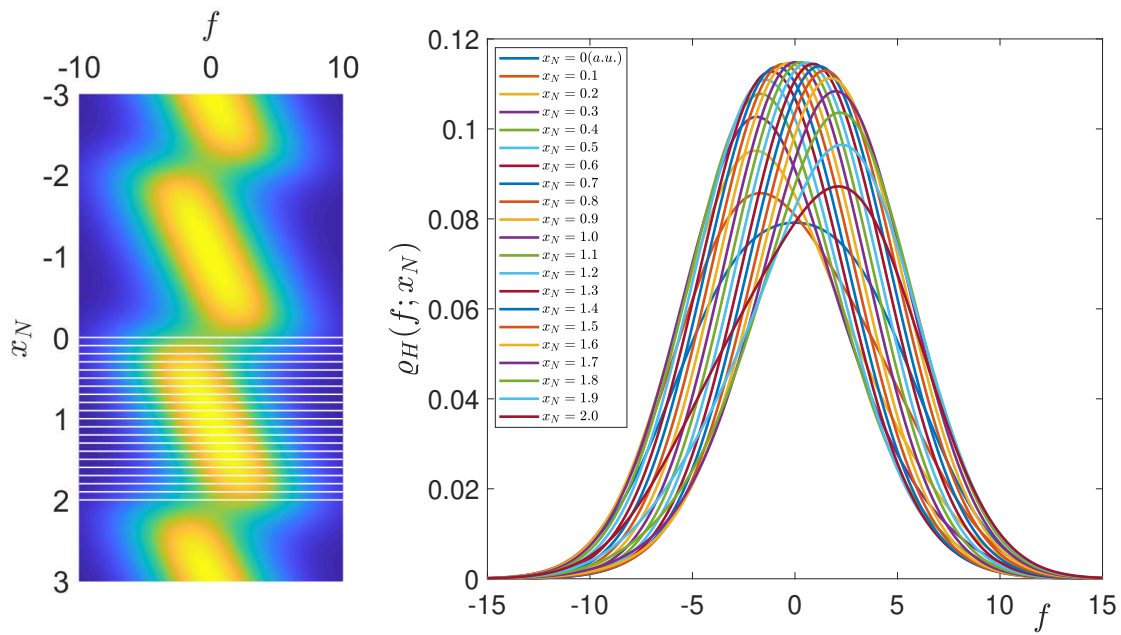


Figure 10. Examples of monomodal curves obtained through the Helmholtz density $\rho_H(f; x_N)$ (see Eq.(54)). On the left panel, the two-dimensional representation of the Helmholtz density is shown with the cuts corresponding to the curves plotted on the right panel. We used $N = 5$, $\ell = 1$ (a.u.), $k = 15$ (a.u.), $k_B T = 1$ (a.u.) and different values of the prescribed position x_N , as indicated in the legend.

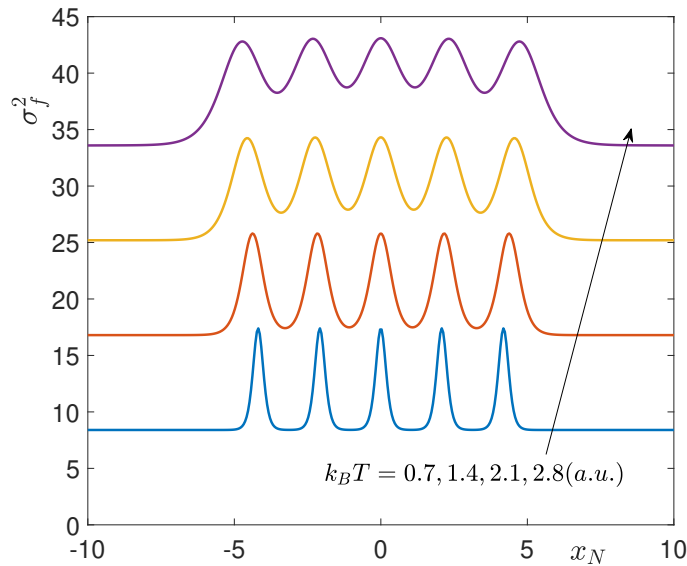


Figure 11. Variance of f obtained by the Helmholtz density $\rho_H(f; x_N)$. As before, we used $N = 5$, $\ell = 1$ (a.u.), $k = 15$ (a.u.) and $k_B T = 0.7, 1.4, 2.1, 2.8$ (a.u.).

369 where we used Eq.(59). As a conclusion, we proved that the classical thermodynamic relation for the
 370 average value of the force is consistent with our development.

371 A numerical application of the results proved in this Section can be found in Figs.8, 9, 10 and 11.
 372 Similarly to the Gibbs analysis, also in this case, we observe that the kinetic part of the probability
 373 density $\rho_H(\dot{f})$ is a simple Gaussian function and therefore we study in more detail the configurational

374 density $q_H(f; x_N)$. Coherently with this planning, in Figs.8 and 9, we show the three-dimensional and
375 the two-dimensional representation of the Helmholtz density as function of f and for a prescribed
376 extension x_N . As before, the results have been obtained for four different temperatures to observe the
377 effects of the thermal agitation on the transition processes. The parameters used in this study are the
378 same already adopted for the Gibbs analysis, namely $N = 5$, $\ell = 1$ (a.u.), $k = 15$ (a.u.) and $k_B T = 0.7, 1.4,$
379 $2.1, 2.8$ (a.u.). We give here a description of the behavior of the system within the Helmholtz ensemble
380 which is exactly dual with respect to the response of the Gibbs ensemble. Indeed, we observe that
381 in spite of the saw-tooth shape of the force-extension response, the probability density of f is quite
382 always monomodal. More precisely, it can be bimodal only with some sets of parameters and only for
383 forces being in the transition region between two peaks of the force-extension curve. Anyway, we can
384 affirm that this density is monomodal in the most cases of practical interest. To better explain this point,
385 we observe that in order to obtain the probability density of f for a prescribed x_N , we have to section
386 the plots in Figs.8 and 9 with a plane parallel to the f -axis and, at the same time, perpendicular to the
387 x_N -axis. By performing this operation, in spite of the complex shape of $q_H(f; x_N)$, we get monomodal
388 functions (with the exceptions discussed above). This can be observed in Fig.10, where we plotted
389 several curves $q_H(f; x_N)$ for different values of the prescribed extension x_N . As before, we remark
390 that the knowledge of the full probability density for the Helmholtz case can be used to determine
391 the expected values of higher order. As an example, in Fig.11 we plotted the variance of the force f ,
392 necessary to impose the extension x_N . Interestingly enough, the variance is an increasing function of
393 the temperature, as expected, and shows some peaks in correspondence to the switching of state of
394 each unit. This is coherent with the general idea that the variance of the physical quantities is larger in
395 proximity to a phase transition. Again, we underline the dual behavior of the Gibbs and Helmholtz
396 ensembles. Indeed, while the variance for the Gibbs case is given by a single peak corresponding to the
397 synchronized transition of the units, for the Helmholtz ensemble we have a peak for each transition,
398 underlying the sequential behavior of this process.

399 6. Discussion and conclusions

400 In this work we considered the comparison of Gibbs (isotensional) and Helmholtz (isometric)
401 ensembles of the (equilibrium) statistical mechanics in the context of the stretching of chains of bistable
402 units. The thermodynamics of the force-extension relations leads to different responses of the two
403 ensembles for small systems, i.e. far from the thermodynamic limit. In particular, the Gibbs response
404 is characterized by a force plateau corresponding to the synchronized transitions of the units, whereas
405 the Helmholtz response can be viewed as a saw-tooth curve representing the sequential transitions
406 of the units. We remark that, when the number of units approaches infinity, the two ensembles
407 become equivalent from the statistical point of view and, therefore, the two Gibbs and Helmholtz
408 force-extension responses become coincident. This general picture, well known in the context of the
409 thermodynamics of small systems, has been widely confirmed experimentally by means of the force
410 spectroscopy methodologies (see Introduction).

411 From the theoretical point of view, this scenario has been complemented here by introducing
412 a method to elaborate the full statistics of these processes at thermodynamic equilibrium, i.e. by
413 the calculation of the probability density of the fluctuating quantities and not only of their average
414 values. The added information is useful to draw full comparisons with experiments and to extract
415 more statistical features valuable from the theoretical point of view. As an example, the knowledge
416 of the complete probability density can be used to evaluate expected values of higher order such as
417 variances, covariances and so forth. Concerning the comparison with experiments, the devices today
418 available to observe the mechanical response of macromolecules (force spectroscopy tweezers) are
419 very refined and allow not only for the measurement of the average values of the main quantities but
420 also to probe the distributions of the same quantities. This can be done by collecting the information
421 of many trajectories of the system and to extract from those data the statistical picture of the system

422 evolution. It means that it is important to update the theoretical devices in order to be able to calculate
423 the probability density of the fluctuating quantities in terms of the deterministic applied ones.

424 Within the Gibbs ensemble, we apply a deterministic force and we measure a stochastic extension.
425 So, we developed here a method to give the probability density of this extension and its rate with
426 respect to the time. On the other hand, within the Helmholtz ensemble, we prescribe a deterministic
427 extension and we measure a stochastic force. Therefore, we obtained in this work the probability
428 density of the force and its time derivative. It is interesting to observe that in both cases these
429 probability densities can be always written in terms of a combination of the two Gibbs and Helmholtz
430 partition functions. This is a typical outcome in statistical mechanics, where all relevant quantities
431 are typically written by means of the partition functions. We remark that, in the case of the number
432 of units approaching infinity, we have the ensemble equivalence as above said. It means that the
433 force-extension curves are the same for both ensembles but the probability densities are not the same
434 because are simply defined on different variables.

435 The results obtained for the specific case of a chain of bistable elements show the emergence of
436 an intriguing duality between the two ensembles. For the isotensional condition, the force-extension
437 curve is monotone with a characteristic force plateau and the density $\varrho(x_N; f)$ is multimodal in the
438 transition region (near $x_N = 0$ and $f = 0$). Conversely, for the isometric condition, the force-extension
439 curve is composed of a series of peaks while the density $\varrho(f; x_N)$ is simply monomodal. This duality
440 is also reflected in the behavior of the variances of these processes. In the Gibbs ensemble we obtained
441 a monomodal variance σ_x^2 with the symmetric peak at $f = 0$, whereas in the Helmholtz ensemble we
442 obtained a multimodal variance σ_f^2 with a peak for each transition value of x_N . Of course, the peaks of
443 variance must be explained through large fluctuations characterizing the switching of the units states
444 (classically, it is typical for the phase transitions).

445 To go further with this analysis, in the next future we will take into consideration the case of
446 bistable elements with two potential wells at different equilibrium length (as considered in this paper)
447 and different equilibrium energy (here we supposed the same energetic level for the two basins). The
448 introduction of the energy difference ΔE between the states will be useful to describe more realistic
449 systems, such as protein domains and other macromolecules of biological origin. Another perspective
450 concerns the consideration of the out-of-equilibrium thermodynamics useful to evaluate the dynamics
451 (the time evolution) of the introduced probability densities, with application to the interpretation of
452 force spectroscopy experiments. To do this, we plan to use our spin variables coupled with a first order
453 dynamics governed by the Kramers rates, which depend on the energy barrier between the wells.

454 To conclude, it is important to underline that the thermodynamics of small systems and
455 bistable-multistable systems is relevant not only for the studies concerning macromolecules and
456 biophysics but only for several applications to nanoscience and nanotechnology, namely for the better
457 understanding of plasticity, hysteretic behaviors and martensitic transformations in solids, micro- and
458 nano-magnetism, ferromagnetic alloys, nano-indented substrates, bistable nanosystems for energy
459 harvesting and transport phenomena in bistable nano-systems such as, e.g., tunnel effect transistors.

460 **Author Contributions:** conceptualization, S. G.; methodology, M. B., F. M., S. G.; software, M. B., F. M.; formal
461 analysis, M. B., F. M., S. G.; writing—original draft preparation, M. B., F. M., S. G.; writing—review and editing, M.
462 B., F. M., S. G.; project administration, S. G.; funding acquisition, S. G.

463 **Funding:** This research was funded by region *Hauts de France* through the project MEPOFIB.

464 **Conflicts of Interest:** The authors declare no conflict of interest. The funders had no role in the design of the
465 study, in the analyses of the problem, in the writing of the manuscript, or in the decision to publish the results.

466 References

- 467 1. Bustamante, C.; Liphardt, J.; Ritort, F. The Nonequilibrium Thermodynamics of Small Systems. *Physics Today*
468 **2005**, *58*, 43, doi: 10.1063/1.2012462.
- 469 2. Dieterich, E.; Camunas-Soler, J.; Ribezzi-Crivellari, M.; Seifert, U.; Ritort, F. Control of force through feedback
470 in small driven systems. *Phys. Rev. E* **2016**, *94*, 012107, doi: 10.1103/PhysRevE.94.012107.

- 471 3. Winkler, R. G. Equivalence of statistical ensembles in stretching single flexible polymers. *Soft Matter* **2010**, *6*,
472 6183, doi: 10.1039/C0SM00488J.
- 473 4. Manca, F.; Giordano, S.; Palla, P. L.; Zucca, R.; Cleri, F.; Colombo L. Elasticity of flexible and semiflexible
474 polymers with extensible bonds in the Gibbs and Helmholtz ensembles. *J. Chem. Phys.* **2012**, *136*, 154906, doi:
475 10.1063/1.4704607.
- 476 5. Manca, F.; Giordano, S.; Palla, P. L.; Cleri, F.; Colombo, L. Response to “Comment on ‘Elasticity of flexible
477 and semiflexible polymers with extensible bonds in the Gibbs and Helmholtz ensembles’” [*J. Chem. Phys.*
478 *138*, 157101 (2013)]. *J. Chem. Phys.* **2013**, *138*, 157102, doi: 10.1063/1.4801656.
- 479 6. Manca, F.; Giordano, S.; Palla, P. L.; Cleri, F. On the equivalence of thermodynamics ensembles for flexible
480 polymer chains. *Phys. A Stat. Mech. its Appl.* **2014**, *395*, 154-170, doi: 10.1016/j.physa.2013.10.042.
- 481 7. Van Kampen, N. G. *Stochastic Processes in Physics and Chemistry*. Elsevier, Amsterdam, 1981.
- 482 8. Risken, H. *The Fokker-Planck equation*. Springer Verlag, Berlin, 1989.
- 483 9. Coffey, W. T.; Kalmykov, Yu. P.; Waldron, J. P. *The Langevin equation*. World Scientific, Singapore, 2004.
- 484 10. Manca, F.; Déjardin, P.-M.; Giordano, S. Statistical mechanics of holonomic systems as a Brownian motion on
485 smooth manifolds, *Annalen der Physik (Berlin)* **2016**, *528*, 381-393, doi: 10.1002/andp.201500221.
- 486 11. Esposito, M.; Van den Broeck, C. Three faces of the second law. I. Master equation formulation. *Phys. Rev. E*
487 **2010**, *82*, 011143, doi: 10.1103/PhysRevE.82.011143.
- 488 12. Van den Broeck, C.; Esposito, M. Three faces of the second law. II. Fokker-Planck formulation. *Phys. Rev. E*
489 **2010**, *82*, 011144, doi: 10.1103/PhysRevE.82.011144.
- 490 13. Tomé, T.; de Oliveira, M. J. Entropy production in irreversible systems described by a Fokker-Planck equation.
491 *Phys. Rev. E* **2010**, *82*, 021120, doi: 10.1103/PhysRevE.82.021120.
- 492 14. Tomé, T.; de Oliveira, M. J. Stochastic approach to equilibrium and nonequilibrium thermodynamics. *Phys.*
493 *Rev. E* **2015**, *91*, 042140, doi: 10.1103/PhysRevE.91.042140.
- 494 15. Jarzynski, C. Nonequilibrium Equality for Free Energy Differences. *Phys. Rev. Lett.* **1997**, *78*, 2690, doi:
495 10.1103/PhysRevLett.78.2690.
- 496 16. Jarzynski, C. Equilibrium free-energy differences from nonequilibrium measurements: A master-equation
497 approach. *Phys. Rev. E* **1997**, *56*, 5018, doi: 10.1103/PhysRevE.56.5018.
- 498 17. Crooks, G. Entropy production fluctuation theorem and the nonequilibrium work relation for free energy
499 differences. *Phys. Rev. E* **1999**, *60*, 2721, doi: 10.1103/PhysRevE.60.2721.
- 500 18. Collin, D.; Ritort, F.; Jarzynski, C.; Smith, S. B.; Tinoco, I.; Bustamante, C. Verification of the Crooks fluctuation
501 theorem and recovery of RNA folding free energies. *Nature* **2005**, *437*, 231-234, doi:10.1038/nature04061.
- 502 19. Jarzynski, C. Comparison of far-from-equilibrium work relations. *Comptes Rendus Physique* **2007**, *8*, 495-506,
503 doi: 10.1016/j.crhy.2007.04.010.
- 504 20. Seifert, U. Stochastic thermodynamics, fluctuation theorems and molecular machines. *Rep. Prog. Phys.* **2012**,
505 *75*, 126001/1-58, doi:10.1088/0034-4885/75/12/126001.
- 506 21. Esposito, M.; Harbola, U.; Mukamel S. Nonequilibrium fluctuations, fluctuation theorems, and counting
507 statistics in quantum systems. *Rev. Mod. Phys.* **2009**, *81*, 1665, doi: 10.1103/RevModPhys.81.1665.
- 508 22. Sekimoto, K. Kinetic Characterization of Heat Bath and the Energetics of Thermal Ratchet Models. *J. Phys.*
509 *Soc. Jpn.* **1997**, *66*, 1234, doi:10.1143/JPSJ.66.1234.
- 510 23. Sekimoto, K. *Stochastic Energetics*. Springer, Berlin 2010.
- 511 24. Wang, Q. A. Maximum path information and the principle of least action for chaotic system, *Chaos, Solitons*
512 *and Fractals* **2004**, *23*, 1253, doi:10.1016/j.chaos.2004.06.046.
- 513 25. Wang, Q. A. Non-quantum uncertainty relations of stochastic dynamics, *Chaos, Solitons and Fractals* **2005**, *26*,
514 1045, doi:10.1016/j.chaos.2005.03.012.
- 515 26. Lucia U. Entropy generation and the Fokker-Planck equation. *Physica A* **2014**, *393*, 256, doi:
516 10.1016/j.physa.2013.09.028.
- 517 27. Lucia, U.; Gervino, G. Fokker-Planck Equation and Thermodynamic System Analysis. *Entropy* **2015**, *17*, 763,
518 doi:10.3390/e17020763.
- 519 28. Lucia, U.; Grazzini, G.; Montrucchio, B.; Grisolia, G.; Borchiellini, R.; Gervino, G.; Castagnoli, C.; Ponzetto,
520 A.; Silvagno, F. Constructal thermodynamics combined with infrared experiments to evaluate temperature
521 differences in cells. *Scientific Report* **2015**, *5*, 11587, doi:10.1038/srep11587.
- 522 29. Perez-Carrasco, R.; Sancho, J. M. Fokker-Planck approach to molecular motors. *EPL* **2010**, *91*, 60001, doi:
523 10.1209/0295-5075/91/60001.

- 524 30. Perez-Carrasco, R.; Sancho, J. M. Molecular motors in conservative and dissipative regimes. *Phys. Rev E*
525 **2011**, *84*, 041915, doi: 10.1103/PhysRevE.84.041915.
- 526 31. Linke, W. A.; Granzier, H.; Kellermayer, M. S. Z.; Eds. *Mechanics of Elastic Biomolecules*. Springer Science,
527 Dordrecht, 2003.
- 528 32. Noy, A.; Ed. *Handbook of Molecular Force Spectroscopy*. Springer Science, New York, 2008.
- 529 33. Strick, T. R. ; Dessinges, M.-N.; Charvin, G.; Dekker, N. H.; Allemand, J.-F.; Bensimon, D.;
530 Croquette, V. Stretching of macromolecules and proteins. *Rep. Progr. Phys.* **2003**, *66*, 1-45, doi:
531 10.1088/0034-4885/66/1/201.
- 532 34. Ritort, F. Single-molecule experiments in biological physics: methods and applications. *J. Phys.: Condens.*
533 *Matter* **2006**, *18*, R531-R583, doi:10.1088/0953-8984/18/32/R01.
- 534 35. Neuman, K. C.; Nagy, A. Single-molecule force spectroscopy: optical tweezers, magnetic tweezers and
535 atomic force microscopy. *Nature Meth.* **2008**, *5*, 491-505, doi: 10.1038/NMETH.1218.
- 536 36. Kumar, S.; Li, M. S. Biomolecules under mechanical force. *Physics Reports* **2010**, *486*, 1-74, doi:
537 10.1016/j.physrep.2009.11.001.
- 538 37. Miller, H.; Zhou, Z.; Shepherd, J.; Wollman A. J. M.; Leake, M. C. Single-molecule techniques in
539 biophysics: a review of the progress in methods and applications. *Rep. Prog. Phys.* **2018**, *81*, 024601,
540 doi: 10.1088/1361-6633/aa8a02.
- 541 38. Yamahata, C.; Collard, D.; Legrand, B.; Takekawa, T.; Kumemura, M.; Hashiguchi, G.; Fujita, H.
542 Silicon Nanotweezers With Subnanometer Resolution for the Micromanipulation of Biomolecules. *J.*
543 *Microelectromech. Syst.* **2008**, *17*, 623-631, doi: 10.1109/JMEMS.2008.922080.
- 544 39. Fisher, T. E.; Oberhauser, A. F.; Carrion-Vazquez, M.; Marszalek, P. E.; Fernandez, J. M. The study
545 of protein mechanics with the atomic force microscope. *Trends Biochem. Sci.* **1999**, *24*, 379-384, doi:
546 10.1016/S0968-0004(99)01453-X.
- 547 40. Li, H.; Oberhauser, A. F.; Fowler, S. B.; Clarke, J.; Fernandez, J. M. Atomic force microscopy reveals the
548 mechanical design of a modular protein. *Proc. Nat. Acad. Sci.* **2000**, *97*, 6527, doi: 10.1073/pnas.120048697.
- 549 41. Imparato, A.; Sbrana, F.; Vassalli, M. Reconstructing the free-energy landscape of a polyprotein by
550 single-molecule experiments. *Europhys Lett.* **2008**, *82*, 58006, doi: 10.1209/0295-5075/82/58006.
- 551 42. Bonin, M.; Zhu, R.; Klaue, Y.; Oberstrass, J.; Oesterschulze, E.; Nellen, W. Analysis of RNA flexibility by
552 scanning force spectroscopy. *Nucleic Acids Res.* **2002**, *30*, e81, doi: 10.1093/nar/gnf080.
- 553 43. Lipfert, J.; Skinner, G. M.; Keegstra, J. M.; Hensgens, T.; Jager, T.; Dulin, D.; Köber, M.; Yu, Z.; Donkers, S. P.;
554 Chou, F.-C.; Das, R.; Dekker, N. H. Double-stranded RNA under force and torque: Similarities to and striking
555 differences from double-stranded DNA. *Proc. Nat. Acad. Sci.* **2014**, *111*, 15408, doi: 10.1073/pnas.1407197111.
- 556 44. Smith, S. B.; Finzi, L.; Bustamante, C. Direct mechanical measurements of the elasticity of single DNA
557 molecules by using magnetic beads. *Science* **1992**, *258*, 1122, doi: 10.1126/science.1439819.
- 558 45. Marko, J. F.; Siggia, E. D. Stretching DNA. *Macromolecules* **1995**, *28*, 8759-8770, doi: 10.1021/ma00130a008.
- 559 46. Smith, S. M.; Cui, Y.; Bustamante, C. Overstretching B-DNA: The Elastic Response of
560 Individual Double-Stranded and Single-Stranded DNA Molecules. *Science* **1996**, *271*, 795, doi:
561 10.1126/science.271.5250.795.
- 562 47. Chaurasiya, K. R.; Paramanathan, T.; McCauley, M. J.; Williams, M. C. Biophysical characterization
563 of DNA binding from single molecule force measurements. *Phys. Life Rev.* **2010**, *7*, 299-341, doi:
564 10.1016/j.plrev.2010.06.001.
- 565 48. Manca, F.; Giordano, S.; Palla, P. L.; Cleri, F. Scaling Shift in Multicracked Fiber Bundles. *Phys. Rev. Lett.* **2014**,
566 *113*, 255501, doi: 10.1103/PhysRevLett.113.255501.
- 567 49. Manca, F.; Giordano, S.; Palla P. L.; Cleri F. Stochastic mechanical degradation of multi-cracked fiber bundles
568 with elastic and viscous interactions. *Euro. Phys. J. E (EPJE)* **2015**, *38*, 44, doi: 10.1140/epje/i2015-15044-1.
- 569 50. Perret, G. ; Lacomberie, T.; Manca, F.; Giordano, S.; Kumemura, M.; Lafitte, N.; Jalabert, L.; Tarhan, M. C.;
570 Lartigau, E. F.; Cleri, F.; Fujita, H.; Collard, D. Real-time mechanical characterization of DNA degradation
571 under therapeutic X-rays and its theoretical modeling. *Microsystems & Nanoengineering (Nature)* **2016**, *2*,
572 16062, doi: 10.1038/micronano.2016.62.
- 573 51. Winkler, R. G. Deformation of semiflexible chains. *J. Chem. Phys.* **2003**, *118*, 2919, doi: 10.1063/1.1537247.
- 574 52. Manca, F.; Giordano, S.; Palla, P. L.; Cleri, F.; Colombo, L. Theory and Monte Carlo simulations for the
575 stretching of flexible and semiflexible single polymer chains under external fields. *J. Chem. Phys.* **2012**, *137*,
576 244907, doi: 10.1063/1.4772656.

- 577 53. Su, T.; Purohit, P. K. Thermomechanics of a heterogeneous fluctuating chain. *J. Mech. Phys. Solids* **2010**, *58*,
578 164, doi: 10.1016/j.jmps.2009.10.007.
- 579 54. Kierfeld, J.; Niamploy, O.; Sa-Yakanit, V.; Lipowsky, R. Stretching of semiflexible polymers with elastic bonds.
580 *Eur. Phys. J. E* **2004**, *14*, 17, doi: 10.1140/epje/i2003-10089-3.
- 581 55. Kramers, H. A. Brownian motion in a field of force and the diffusion model of chemical reactions. *Physica*
582 *(The Hague)* **1940**, *7*, 284-304, doi: 10.1016/S0031-8914(40)90098-2.
- 583 56. Dudko, O. K. Decoding the mechanical fingerprints of biomolecules. *Quarterly Reviews of Biophysics* **2016** *49*,
584 1-14, doi:10.1017/S0033583515000220.
- 585 57. Manca, F.; Pincet, F.; Truskinovsky, L.; Rothman, J. E.; Foret, L.; Caruel M. SNARE machinery is optimized
586 for ultrafast fusion. *PNAS* **2019**, doi:10.1073/pnas.1820394116.
- 587 58. Rief, M.; Fernandez, J. M.; Gaub, H. E. Elastically Coupled Two-Level Systems as a Model for Biopolymer
588 Extensibility. *Phys. Rev. Lett.* **1998**, *81*, 4764, doi: 10.1103/PhysRevLett.81.4764.
- 589 59. Kreuzer, H. J.; Payne, S. H. Stretching a macromolecule in an atomic force microscope: Statistical mechanical
590 analysis. *Phys. Rev. E* **2001**, *63*, 021906, doi: 10.1103/PhysRevE.63.021906.
- 591 60. Manca, F.; Giordano, S.; Palla, P. L.; Cleri, F.; Colombo, L. Two-state theory of single-molecule stretching
592 experiments. *Phys. Rev. E*, **2013** *87*, 032705, doi: 10.1103/PhysRevE.87.032705.
- 593 61. Giordano, S. Helmholtz and Gibbs ensembles, thermodynamic limit and bistability in polymer lattice models.
594 *Continuum Mech. Thermodyn.* **2018**, *30*, 459, doi: 10.1007/s00161-017-0615-5.
- 595 62. Bosaeus, N.; El-Sagheer, A. H.; Brown, T.; Smith, S. B.; Akerman, B.; Bustamante, C.; Nordén, B. Tension
596 induces a base-paired overstretched DNA conformation. *Proc. Natl. Acad. Sci. USA* **2012**, *109*, 15179, doi:
597 10.1073/pnas.1213172109.
- 598 63. Wang, J.; Kouznetsova, T. B.; Boulatov, R.; Craig, S. L. Mechanical gating of a mechanochemical reaction
599 cascade. *Nature Comm.* **2016**, *7*, 13433, doi: 10.1038/ncomms13433.
- 600 64. Cocco, S.; Yan, J.; Léger, J. F.; Chatenay, D.; Marko, J. F. Overstretching and force-driven strand separation of
601 double-helix DNA. *Phys. Rev. E* **2004**, *70*, 011910, doi: 10.1103/PhysRevE.70.011910.
- 602 65. Cocco, S.; Marko, J. F.; Monasson, R.; Sarkar, A.; Yan, J. Slow nucleic acid unzipping kinetics from
603 sequence-defined barriers. *Eur. Phys. J. E* **2003**, *10*, 249, doi: 10.1140/epje/e2003-00019-8.
- 604 66. Rief, M.; Oesterhelt, F.; Heymann, B.; Gaub, H. E. Single Molecule Force Spectroscopy on Polysaccharides by
605 Atomic Force Microscopy. *Science* **1997**, *275*, 1295, doi: 10.1126/science.275.5304.1295.
- 606 67. Hanke, F.; Kreuzer, H. J. Conformational transitions in single polymer molecules modeled with a complete
607 energy landscape: continuous two-state model. *Eur. Phys. J. E* **2007**, *22*, 163, doi: 10.1140/epje/e2007-00027-8.
- 608 68. Rief, M.; Gautel, M.; Oesterhelt, F.; Fernandez, J. M.; Gaub, H. E. Reversible unfolding of individual titin
609 immunoglobulin domains by AFM. *Science* **1997**, *276*, 1109, doi: 10.1126/science.276.5315.1109.
- 610 69. Staple, D. B.; Payne, S. H.; Reddin, A. L. C.; Kreuzer, H. J. Stretching and unfolding of
611 multidomain biopolymers: a statistical mechanics theory of titin. *Phys. Biol.* **2009**, *6*, 025005, doi:
612 10.1088/1478-3975/6/2/025005.
- 613 70. Prados, A.; Carpio, A.; Bonilla, L. L. Sawtooth patterns in force-extension curves of biomolecules: An
614 equilibrium-statistical-mechanics theory. *Phys. Rev. E* **2013**, *88*, 012704, doi: 10.1103/PhysRevE.88.012704.
- 615 71. Bonilla, L. L.; Carpio, A.; Prados, A. Theory of force-extension curves for modular proteins and DNA
616 hairpins. *Phys. Rev. E* **2015**, *91*, 052712, doi: 10.1103/PhysRevE.91.052712.
- 617 72. De Tommasi, D.; Millardi, N.; Puglisi, G.; Saccomandi, G. An energetic model for macromolecules unfolding
618 in stretching experiments. *J. R. Soc. Interface* **2013**, *10*, 20130651, doi: 10.1098/rsif.2013.0651.
- 619 73. Makarov, D. E. A Theoretical Model for the Mechanical Unfolding of Repeat Proteins. *Biophys. J.* **2009**, *96*,
620 2160, doi: 10.1016/j.bpj.2008.12.3899.
- 621 74. Giordano, S. Spin variable approach for the statistical mechanics of folding and unfolding chains. *Soft Matter*
622 **2017**, *13*, 6877-6893, doi: 10.1039/c7sm00882a.
- 623 75. Benedito, M.; Giordano, S. Thermodynamics of small systems with conformational transitions: the case of
624 two-state freely jointed chains with extensible units. *J. Chem. Phys.* **2018**, *149*, 054901, doi: 10.1063/1.5026386.
- 625 76. Benedito, M.; Giordano, S. Isotensional and isometric force-extension response of chains with bistable units
626 and Ising interactions. *Phys. Rev. E (Editors' Suggestion)* **2018**, *98*, 052146, doi: 10.1103/PhysRevE.98.052146.
- 627 77. Caruel, M.; Allain, J. M.; Truskinovsky, L. Muscle as a Metamaterial Operating Near a Critical Point. *Phys.*
628 *Rev. Lett.* **2013**, *110*, 248103, doi: 10.1103/PhysRevLett.110.248103.

- 629 78. Caruel, M.; Truskinovsky, L. Statistical mechanics of the Huxley-Simmons model. *Phys. Rev. E* **2016**, *93*,
630 062407, doi: 10.1103/PhysRevE.93.062407.
- 631 79. Ericksen, J. L. Equilibrium of bars. *J. Elasticity* **1975**, *5*, 191, doi: 10.1007/BF00126984.
- 632 80. Müller, I.; Villaggio, P. A model for an elastic-plastic body. *Arch. Rational Mech. Anal.* **1977**, *65*, 25, doi:
633 10.1007/BF00289355.
- 634 81. Fedelich, B.; Zanzotto, G. Hysteresis in discrete systems of possibly interacting elements with a double-well
635 energy. *J. Nonlinear Sci.* **1992**, *2*, 319-342, doi: 10.1007/BF01208928.
- 636 82. Puglisi, G.; Truskinovsky, L. Thermodynamics of rate-independent plasticity. *J. Mech. Phys. Sol.* **2005**, *53*, 655,
637 doi: 10.1016/j.jmps.2004.08.004.
- 638 83. Caruel, M.; Allain, J.-M.; Truskinovsky, L. Mechanics of collective unfolding. *J. Mech. Phys. Sol.* **2015**, *76*, 237,
639 doi: 10.1016/j.jmps.2014.11.010.
- 640 84. Efendiev, Y. R.; Truskinovsky, L. Thermalization of a driven bi-stable FPU chain. *Continuum Mech. Thermodyn.*
641 **2010**, *22*, 679, doi: 10.1007/s00161-010-0166-5.
- 642 85. Mielke, A.; Truskinovsky, L. From Discrete Visco-Elasticity to Continuum Rate-Independent Plasticity:
643 Rigorous Results. *Arch. Rational Mech. Anal.* **2012**, *203*, 577-619, doi: 10.1007/s00205-011-0460-9.
- 644 86. Benichou, I.; Givli, S. Structures undergoing discrete phase transformation. *J. Mech. Phys. Sol.* **2013**, *61*, 94,
645 doi: 10.1016/j.jmps.2012.08.009.
- 646 87. Restrepo, D.; Mankame, N. D.; Zavattieri, P. D. Phase transforming cellular materials. *Extr. Mech. Lett.* **2015**,
647 *4*, 52-60, doi: 10.1016/j.eml.2015.08.001.
- 648 88. Frazier, M. J.; Kochmann, D. M. Band gap transmission in periodic bistable mechanical systems. *J. Sound*
649 *and Vib.* **2017**, *388*, 315-326, doi: 10.1016/j.jsv.2016.10.041.
- 650 89. Katz, S.; Givli, S. Solitary waves in a bistable lattice. *Extr. Mech. Lett.* **2018**, *22*, 106-111, doi:
651 10.1016/j.eml.2018.06.003.
- 652 90. Hwang, M.; Arrieta, A. F. Nonlinear dynamics of bistable lattices with defects. *Proc. SPIE, Health Monitoring*
653 *of Structural and Biological Systems* **2017**, 101701A, doi: 10.1117/12.2263609.
- 654 91. Hwang, M.; Arrieta, A. F. Response invariance in a lattice of bistable elements with elastic interactions.
655 *Proc. SPIE 10595, Active and Passive Smart Structures and Integrated Systems XII* **2018**, 105950X, doi:
656 10.1117/12.2303422.
- 657 92. Harne, R. L.; Schoemaker, M. E.; Wang, K. W. Multistable chain for ocean wave vibration energy
658 harvesting. *Proc. SPIE 9057, Active and Passive Smart Structures and Integrated Systems* **2014**, 90570B, doi:
659 10.1117/12.2044267.

660 © 2019 by the authors. Submitted to *Inventions* for possible open access publication
661 under the terms and conditions of the Creative Commons Attribution (CC BY) license
662 (<http://creativecommons.org/licenses/by/4.0/>).